DOT/FAA/TC-20/7

Federal Aviation Administration
William J. Hughes Technical Center
Aviation Research Division
Atlantic City International Airport
New Jersey 08405

Research Studies for Notched Laminates Under Out-of-Plane Loading

September 2020

Final report

U.S. Department of Transportation
Federal Aviation Administration

NOTICE

This report is available at the Federal Aviation Administration William J. Hughes Technical Center's Full-Text Technical Reports page: actlibrary.tc.faa.gov in Adobe Acrobat portable document format (PDF).

Technical Report Documentation Page

Form DOT F 1700.7 (8-72) Reproduction of completed page authorized

1. Report No.	2. Government Accession No.	3. Recipient's Catalog No.
DOT/FAA/TC-20/7		

4. Title and Subtitle	5. Report Date
Research Studies for Notched Laminates Under Out-of-Plane Loading	September 2020
	6. Performing Organization Code

7. Author(s)	8. Performing Organization Report No.
D. Plechaty, K. Carpenter, T. McKinley, J.P. Parmigiani	

9. Performing Organization Name and Address	10. Work Unit No. (TRAIS)
School of MIME Oregon State University Corvallis, OR 97331	11. Contract or Grant No.

12. Sponsoring Agency Name and Address	13. Type of Report and Period Covered
U.S. Department of Transportation Federal Aviation Administration Air Traffic Organization NextGen & Operations Planning Office of Research and Technology Development Washington, DC 20591	Final Report
	14. Sponsoring Agency Code

15. Supplementary Notes

The FAA William J. Hughes Technical Center Aviation Research Division Technical Monitor was Lynn Pham.

16. Abstract

As composite materials become more prevalent in aircraft structures, damage tolerance requirements for these materials must be met. Predicting failure in notched laminates has been studied rigorously—with the main focus being the response to in-plane tension, compression, or shear. Out-of-plane bending, twisting, or shear has not been investigated as thoroughly, although it is a common loading situation for configured aircraft structures, subjected to combined loads. An incomplete understanding of the response to out-of-plane loads may result in excessively conservative designs of aircraft, driving up the amount of material needed. The subsequent increase in weight and overall cost of the aircraft is undesirable and provides an opportunity for improvement. In partnership with The Boeing Company, Oregon State University (OSU) investigated the failure modes of laminates in out-of-plane loading and evaluated the capability of current analysis and modeling techniques to predict failure. This effort has been explored in three different OSU research studies documented in this report: 1) A sensitivity study of the Hashin criteria for modeling progressive damage explored which of 10 material properties were most significant for some simple laminate layups. Findings could have a significant impact on selection of test specimens for Hashin property determination, characterization, and calibration; 2) Experimental and analytical investigations of edge-notched carbon fiber panels under mode III loading characterized the material response. Future sensitivity studies should evaluate other more complex laminate layups characteristic of wing and fuselage composite structures. The experimental failure load of different more complex ply layups was measured and Digital Image Correlation was used to capture the strain field measurements. ABAQUS/Standard and ABAQUS/Explicit were able to predict experimental maximum loads within 20%. ABAQUS/Explicit required excessively long run times and produced noisy solutions. ABAQUS/Standard with Helius multi-continuum theory showed potential, although the instant degradation technique led to convergence failures prior to obtaining maximum loads; 3) The final study investigated matrix compression in carbon fiber panels. Finite element software was used to select a specimen geometry that exhibited matrix compression failure and used a simple experimental setup. The Stepped Compact Compression specimen was found to be suitable. After the specimen was chosen, experiments were conducted to characterize matrix compression damage. For compact compression test specimens, it was found that shear cracks through the thickness of the material were the primary failure mechanism, followed by tensile failure at the edge opposite the crack.

17. Key Words	18. Distribution Statement
Composites, Damage tolerance, Notched laminates, Out-of-plane loading, Analysis, Modeling	This document is available to the U.S. public through the National Technical Information Service (NTIS), Springfield, Virginia 22161. This document is also available from the Federal Aviation Administration William J. Hughes Technical Center at actlibrary.tc.faa.gov.

19. Security Classif. (of this report)	20. Security Classif. (of this page)	21. No. of Pages	22. Price
Unclassified	Unclassified	57	

Acknowledgements

This work was funded through the FAA Joint Advanced Materials and Structures Center of Excellence, with Lynn Pham as the project monitor, and by The Boeing Company. The authors wish to express their appreciation for technical guidance provided by Kazbek Karayev and Gerald Mabson of Boeing and Larry Ilcewicz of the FAA.

Contents

Figures

Tables

Acronyms

Acronym	Definition
4PB	Four-point bend
CC	Compact compression
CFRP	Carbon fiber reinforced polymer
CNC	Center-notched compression
DIC	Digital image correlation
ENC	Edge notch compression
FAA	Federal Aviation Administration
FE	Finite element
FEA	Finite element analysis
MCT	Multi-continuum theory
OSU	Oregon State University
SC8R	8-node reduced-integration shell element
TENC	Tapered edge notch compression

Executive summary

As composite materials become more prevalent in aircraft structures, damage tolerance requirements for these materials must be met. Predicting failure in notched laminates has been studied rigorously—with the main focus being the response to in-plane tension, compression, or shear. Out-of-plane bending, twisting, or shear has not been investigated as thoroughly, although it is a common loading situation for aircraft structures. An incomplete understanding of the response to out-of-plane loads may result in excessively conservative designs of aircraft, driving up the amount of material needed. The subsequent increase in weight and overall cost of the aircraft is undesirable and provides an opportunity for improvement. In partnership with The Boeing Company, Oregon State University (OSU) investigated the failure modes of laminates in out-of-plane loading and evaluated the capability of current analysis and modeling techniques to predict failure. This effort has been explored in three different OSU research studies.

1. A sensitivity study using the Hashin criteria for modeling progressive damage explored which of the 10 material properties required in the Hashin model were most significant in predicting failure loads. By means of a fractional factorial analysis, the most significant material properties were determined. It was found that, depending on ply orientation and loading scenario, not all 10 of the required material properties are significant. In some cases, as many as four properties were significant; in other cases, only one. Findings could have a significant impact on selection of test specimens for Hashin property determination, characterization, and calibration.
2. An experimental investigation of edge-notched carbon fiber reinforced polymer (CFRP) panels exposed to mode III characterized the material response of composites under out-of-plane shear loading. The failure load of different ply layups was measured, and digital image correlation (DIC) was used to capture the strain field measurements. The strain fields were compared to finite element analysis (FEA) results using the commercial software ABAQUS®. It was determined that under mode III shear, the composite experienced a region of tensile strain concentration and a region of compressive strain concentration. It was also determined that the resulting increases in the tensile strain concentration areas signified initial damage in panels having fewer zero-degree plies. However, increases in the compressive strain concentration areas occurred for panels with more zero-degree plies. It was also ascertained that the ABAQUS simulation results were significantly different from the DIC-measured strain values. Differences between simulation and measured strain values were up to 60% higher and 40% lower for low loads, and there were as much as a 100% difference under greater loads. A further study investigated the ability of different ABAQUS packages to model composites exposed to

mode III out-of-plane shear in two situations: prior to the onset of visible damage and for the progression of damage. ABAQUS/Standard was found to be an acceptable tool to model mode III loading in composites prior to damage initiation. Although the FEA did not align directly with experimental results for mode III, it provided a good estimate. For progressive damage, ABAQUS/Standard and ABAQUS/Explicit were able to predict experimental maximum loads within 20%. ABAQUS/Explicit required excessively long run times and produced noisy solutions. ABAQUS/Standard with Helius multi-continuum theory showed potential, although the instant degradation technique led to convergence failures prior to obtaining maximum loads.

3. The final study investigated matrix compression in CFRP panels. FE software was used to select a specimen geometry that exhibited matrix compression failure and used a simple experimental setup. The Stepped Compact Compression specimen was found to be suitable. After the specimen was chosen, experiments were conducted to characterize matrix compression damage. For compact compression test specimens, it was found that shear cracks through the thickness of the material were the primary failure mechanism, followed by tensile failure at the edge opposite the crack.

1 Introduction

Damage tolerance requirements on aircraft structures have a significant influence on the design of aircraft using composite materials. Predicting failure in notched laminates has been investigated repeatedly; the focus of these studies has been, in general, on in-plane tension, compression, or shear. However, out-of-plane loading is a common scenario on these structures and has not been investigated as thoroughly. Therefore, the response of notched laminates under out-of-plane loads is not well understood. This uncertainty can lead to unnecessarily conservative design, driving up the cost, weight, and overall efficiency in the manufacturing and performance of aircraft.

The designs of composite aircraft structures need analysis techniques that are effective and reliable for out-of-plane loading. Unfortunately, developing these techniques is complicated because laminates do not experience uniform strain throughout their thickness, which may lead to progressive damage development up to final failure. Additionally, in homogenous metal structures, all failure modes (I, II, and III) can occur simultaneously at a notch tip; in laminates, it can be expected to be even more complex. Simulating this behavior in models will be difficult, and the analysis techniques requires experimental support, for which there are little test data currently available.

The primary goal of this research was to evaluate analysis techniques for composites exposed to out-of-plane loading. These techniques should be accurate, efficient, and suitable for implementation into current design methodology. The models must be validated through tests on small samples then large configured structures. The focus on this research involved investigations on simple carbon fiber reinforced polymer (CFRP) composite panels exposed to out-of-plane loading. The modes of failure of laminates were determined, and currently existing analysis techniques were evaluated for their capability to predict the failure.

Notched laminates were explored through three studies:

1. A sensitivity study on the Hashin damage model for progressive failure of laminates under out-of-plane bending and tension loads
2. Experimental and analytical studies of laminates subjected to mode III: out-of-plane shear.
3. Preliminary investigation of matrix compression through FEA and experiment

The sensitivity study of the Hashin criteria for modeling progressive damage explored which of the 10 material properties required for the Hashin model were most significant in predicting

failure loads. By means of a fractional factorial analysis, the most significant material properties were determined.

The study of edge-notched CFRP panels exposed to mode III characterized the material response of composites under out-of-plane shear loading. The failure load of different ply layups was measured, and digital image correlation (DIC) was used for strain field measurements and comparison to FEA results. Also investigated in this study was the ability of different ABAQUS packages to model composites exposed to mode III out-of-plane shear in two situations: 1) prior to the onset of visible damage and 2) for the progression of damage.

The final study investigated matrix compression in CFRP panels. Finite element (FE) software was used to select a specimen that exhibited matrix compression failure and required a simple experimental setup. After the specimen was chosen, experiments were run to classify matrix compression damage.

2 Sensitivity study of Hashin damage model of progressive failure under tension and out-of-plane bending

The Hashin damage model is based on the work of Matzenmiler et al. [1], Hashin and Rotem [2], Hashin [3], and Camanho and Davila [4]. This model is used to calculate the load of failure initiation in notched CFRP panels and requires specific material properties. Table 1 defines the material properties required for linear elasticity and the Hashin model, including nominal values from the work of Wong et al. [5].

Table 1. Material properties for linear elasticity and Hashin progressive damage model, with nominal values

Material Property		Definition	Value
Linear elastic material properties	E_1	Longitudinal Young's modulus	131.9 GPa
	E_2	Transverse Young's modulus	9.51 GPa
	ν_{12}, ν_{13}, ν_{23}	Poisson's ratio	0.326, 0.341, 0.485
	G_{12}, G_{13}, G_{23}	Shear modulus	5.27, 7.03, 3.39 GPa
Hashin model material properties	X^T	Tensile strength in the direction parallel to the fibers	1328 MPa
	X^C	Compressive strength in the direction parallel to the fibers	1064 MPa
	Y^T	Tensile strength in the in-plane direction, normal to the fibers	70.9 MPa
	Y^C	Compressive strength in the in-plane direction, normal to the fibers	221 MPa
	S^L	Longitudinal (in-plane) shear strength	71.2 MPa
	S^T	Transverse shear strength	94.5 MPa
	G_{ft}	Area under stress-displacement curve for fiber tension	2.0 N/mm
	G_{fc}	Area under stress-displacement curve for fiber compression	2.0 N/mm
	G_{mt}	Area under stress-displacement curve for matrix tension	0.33 N/mm
	G_{mc}	Area under stress-displacement curve for matrix compression	0.33 N/mm

In the Hashin damage model, damage initiates and can progress through four possible modes: 1) fiber tension, 2) fiber compression, 3) matrix tension, and 4) matrix compression. The onset of damage occurs when one of the Hashin criteria are satisfied. The criterion uses a comparison between the stress states and associated material strength properties. The damage initiation criteria are listed in Table 2, where $\hat{\sigma}_{11}$, $\hat{\sigma}_{22}$, and $\hat{\tau}_{12}$ are the in-plane normal and shear stresses,

respectively, and α determines the contribution of shear stress to the fiber tension mode of failure, which Hashin [3] suggests to be unity.

Table 2. Damage initiation criteria specified by the Hashin damage model

Damage Mode	Initiation Criteria
Fiber Tension	$\left(\frac{\hat{\sigma}_{11}}{X^T}\right)^2 + \alpha\left(\frac{\hat{\tau}_{12}}{S^L}\right)^2 = 1$ (1)
Fiber Compression	$\left(\frac{\hat{\sigma}_{11}}{X^C}\right)^2 = 1$ (2)
Matrix Tension	$\left(\frac{\hat{\sigma}_{22}}{Y^T}\right)^2 + \left(\frac{\hat{\tau}_{12}}{S^L}\right)^2 = 1$ (3)
Matrix Compression	$\left(\frac{\hat{\sigma}_{22}}{2S^T}\right)^2 + \left[\left(\frac{Y^C}{2S^T}\right)^2 - 1\right]\frac{\hat{\sigma}_{22}}{Y^C} + \left(\frac{\hat{\tau}_{12}}{S^L}\right)^2 = 1$ (4)

The Hashin properties are generally determined through coupon testing and analysis. Particularly for the Hashin properties, in many cases, the uncertainty in these values is high. However, for a given loading and ply lay-up it is possible than not all of the Hashin properties have a significant effect on calculated load-carrying ability. Knowing which are most significant for a given loading and ply lay-up is advantageous in several ways. First, it allows an overall assessment of the effect of varying uncertainty in Hashin properties (i.e. the uncertainty of some properties is greater than the uncertainty of others) on the calculated load-carrying ability. For example, if the properties having the greatest effect on the calculated load-carrying ability also have the least uncertainty one can have greater confidence in the results. Second, knowing which properties are most significant can guide the allocation of resources in property determination (i.e. only expend resource to more-accurately determine the values of the material properties having a significant effect on the calculated parameters). Finally, if for a given loading or lay-up only one property is found to be significant, then that loading/lay-up combination could be used to determine that property. In the remainder of this report the term *Sensitivity Study* will be used to refer to a determination of the significance of each of the ten Hashin parameters on calculated load-carrying ability.

Kennedy et al. conducted a sensitivity study of Hashin properties [6]. Geometry was a center-notched CFRP panel having a layup with typical aerospace orientations (i.e. having 0, +45, -45 and 90 degree plies), specifically $[45/0/0/45/90/-45/0/0/45/90]_s$. Loading was out-of-plane bending. Their results showed that G_{ft}, X^T, G_{fc}, and X^C were significant in both the stiff and soft direction of the laminate. They concluded that the failure of notched laminates under bending is dominated by the ply properties in the fiber direction. Also, large changes in these properties ($\pm$20%) tend to produce small changes in failure load ($<\pm$7%).

The study described in this report extends this prior work through the inclusion of both tension and out-of-plane bending and the consideration of five simple layups. Each of these five layups consist of no-more-than two of the following orientations: 0°, -45°, 45°, and 90°. Consideration of such simple layups enables identification of fundamental trends is behavior and identifying loading/lay-up combinations useful for determining, characterizing, and calibrating Hashin material properties [7].

2.1 FE model and experimental setup

As damage propagates, the material loses its stiffness and load-carrying ability, resulting in strain-softening behavior. In FEA models, the strain-softening behavior can cause problematic mesh-dependency. The commercial software, ABAQUS, uses a stress-displacement law for each of the four modes, instead of the usual stress-strain law, to address the mesh dependency issue. Additionally, use of the stress-displacement curves is used in determining the displacement at failure by means of the fracture energy, a material property that must be determined experimentally.

The specimen geometry, loading arrangements, and FE mesh selected for this study were chosen based on the work of Kennedy et al. [6] and Arias [8]. Their exploration consisted of a series of FEA models of CFRP center-notched panels under out-of-plane bending and was shown to have good agreement with experimental results.

2.1.1 FEA model

The commercial FEA program, ABAQUS, was used for this study. It was determined by Kennedy et al. [6] that thin, center-notched panels loaded under out-of-plane bending would fail without delamination effects, and FE models need not include these effects. Therefore, if the laminates have fewer than 20 plies, conventional shell elements may be used. With the ply layups used in this work having eight plies, it was deemed sufficient to use conventional shell elements.

Each model element contained three integration points through the thickness of each lamina. The mesh was refined near the notch (where damage was most common) and coarse near the edges, as seen in Figure 1. Mesh refinement efforts produced a high density of equally sized elements surrounding the notch, which is critical in capturing the stress concentration gradient and subsequent damage near the notch tip.

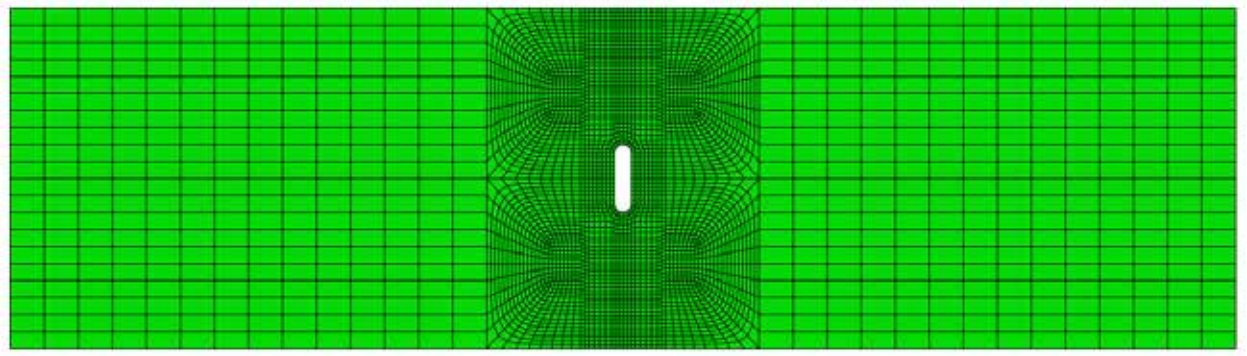

Figure 1. Mesh of FE model

The element size near the notch tip was determined by selecting the coarsest mesh that converged for models using an elastic solution without damage. The model consisted of 3868 elements, approximately 1.59 mm near the notch, and 5.08 mm by 12.7 mm outside of the refinement zone.

The panel was loaded with either in-plane tension (using a displacement boundary condition along the panel-width edges) or out-of-plane bending (using a displacement boundary condition at four points parallel to the notch). Displacements were applied until a maximum load was clearly identified (i.e., damage had progressed such that increased deformation occurred at decreasing loads).

2.1.2 Specimen geometry

The panel geometry consisted of a 127-mm-wide, 457.2-mm-long rectangle, 0.15-mm thick, with a 25.4 mm straight-sided center notch having end radii of 3.175 mm (see Figure 1). The notch was aligned parallel to the panel width.

Ply orientation can have a significant effect on the mechanical behavior of CFRP laminates. Therefore, several different ply layups were studied: five layups for in-plane tension and three layups (layups 1–3) for the out-of-plane bending case. Table 3 shows the layup configuration, where 0° is perpendicular to the notch, and 90° is parallel to the notch.

Table 3. Ply layup orientation

Layup 1	Layup 2	Layup 3	Layup 4	Layup 5
0°	0°	-45°	90°	90°
0°	45°	45°	-45°	90°
0°	0°	-45°	90°	90°
0°	45°	45°	-45°	90°
0°	45°	45°	-45°	90°
0°	0°	-45°	90°	90°
0°	45°	45°	-45°	90°
0°	0°	-45°	90°	90°

2.1.3 Design of experiments

The study methodology used a two-level fractional factorial experiment design and analysis. In a two-level fractional factorial experiment, each factor is given a high and a low value, and not all factor combinations are tested. Fractional factorial designs can have different resolutions, which reflect the type of effects that are coupled, or "aliased." For example, a resolution III design has main effects aliased with two-factor and higher order interactions, and a resolution IV design has main effects aliased with three-factor and higher order interactions.

A "main effect" is the effect on the response variable by changing the level of a single factor, and "interactions" refer to the difference in the effect of one factor at varying levels of another factor (or combination of factors). By not testing all possible factor combinations, and therefore having fewer experiments, the result is aliasing.

When a small fraction of the experimental factors dominates the effects of the response, the fractional factorial experiment is effective, and aliasing can be resolved with "design projection." Design projection uses either additional experimentation with only the significant factors, or eliminates the non-significant factors and uses the same experimental data as the results of a non-fractional experiment with fewer factors.

Design projection to resolve aliasing, if only half of the original runs are desired, require a 2^{k-p} factorial experiment, where k is the number of factors, and p indicates the size of the fraction of the full factorial.

Fractional factorial designs found in Montgomery [9] were used. A 2^{10-5} design (Resolution III) was used for tension and a 2^{10-4} design (Resolution IV) for bending. A greater resolution was used for bending due to its inherently greater internal-loading complexity. In each of the designs, the two levels used were set at 20% above and below the nominal value of a particular factor. All material properties originated from the work of Wong et al. [5] and are listed in Table 1.

Effect estimates (the estimated difference in the response between high and low levels of a factor or interaction) can be computed from the experimental results by comparing treatment responses [9]. A normal probability plot of effect estimates can identify which factors are significant to the response. However, this is based on the assumption that a reasonable mathematical model of the response is a linear function of the factor levels, with a normally distributed "error" term. If there is negligible effect of a factor or interaction as it changes from a low to a high value, the estimate is the error term. If the effect is significant, the estimate will be a different normally distributed random variable.

When all of the effect estimates are shown on a normal probability plot, those factors with negligible effect will fall on the same straight line, in contrast to those factors with large effects.

2.2 Sensitivity of Hashin criteria to model failure: in-plane tension

The in-plane tension case consisted of five different ply layups. Results were very similar for both ply layups 1 and 2 with normal probability plots indicated a single significant factor effect. This effect signified the aliased sum of the effects of the fiber tensile strength, X^T, and the interaction between fiber compressive strength, X^C, and matrix compressive fracture energy, G_{mc}. Resolving this aliasing was undertaken by a subsequent 2^3 experiment, using only X^T, X^C, and G_{mc} for each ply layup. It was found that only X^T was significant in both ply layups 1 and 2 for the in-plane tension case. The normal probability plot of the effect estimates for layup 1 is shown in Figure 2 [6, 10]. The outliner is the data point at an effect of approximately 3000 N corresponding to either the main factor of X_T, or the interaction between X_C and G_{mc}.

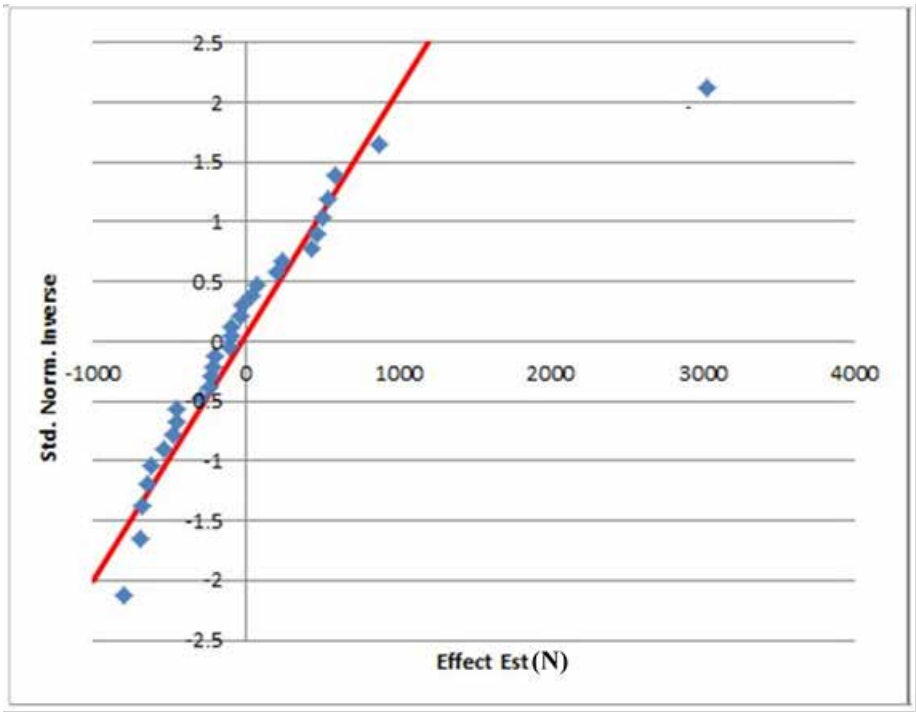

Figure 2. Normal probability plot of effects for layup 1 in tension

Figure 3 [6, 10] shows subsequent 2^3 factorial analysis for layup 1. The outliner is the data point at an effect of approximately 2700 N which identifies only main effect of factor X^T as significant. The normal probability plots for other layups are analogous.

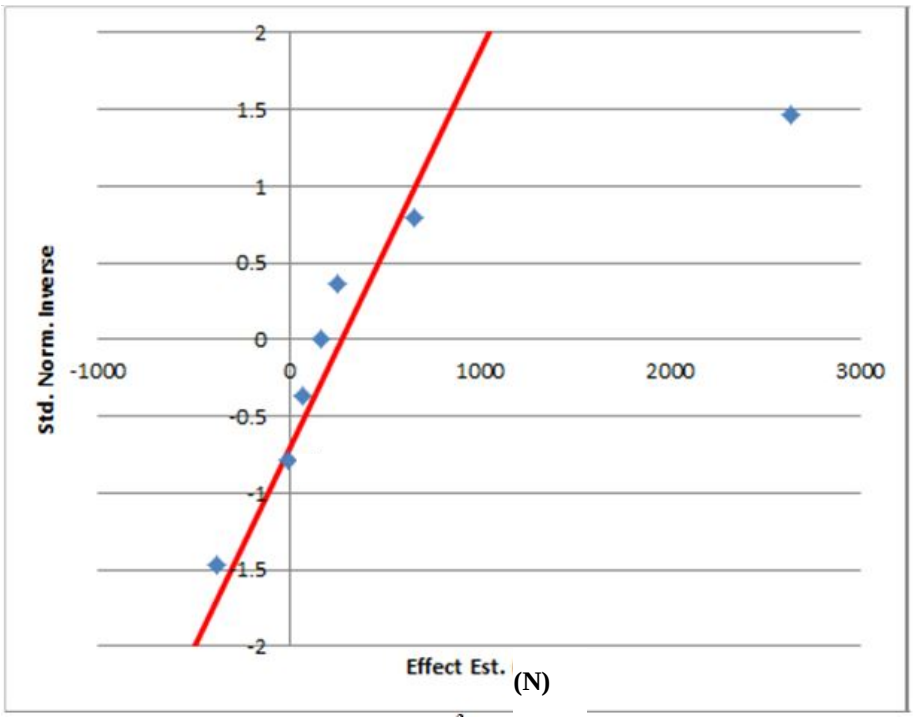

Figure 3. Normal probability plot of 2^3 factorial analysis for layup 1 in tension

Ply layup 3 identified three significant factor effects from the normal probability plot: the longitudinal shear strength (S^L) effect; the aliased sum of X^T, X^C, and G_{mc}; the interaction between X^T and S^L and aliased with the interaction between matrix compressive strength (Y^C) and transverse shear strength (S^T). To resolve this aliasing, a subsequent 2^{6-1} experiment was conducted. Three identified significant factor effects in order of significance were S^L, X^T, and the interaction between S^L and X^T.

Ply layup 4 revealed four significant effects. In order of significance, they were the effect of longitudinal shear strength (Y^T); the effect of S^L; the effect of the interaction of Y^T and S^L aliased with the effect of the interaction of Y^C and Y^T; and the effect of G_{mt} aliased with the interaction of S^T and G_{mc}. To resolve this aliasing, a subsequent 2^{7-2} experiment (Resolution IV) was conducted. Results showed the significant factor effects to be Y^T, S^L, and G_{mt}, and the interaction between Y^T and S^L.

Finally, ply layup 5 had one significant effect. This effect was not aliased with a two-factor interaction and therefore identified the single material property Y^T to be significant. The significant material properties and effects for each layup under tension are summarized in Table 4.

Table 4. Summary of significant material properties and their effect on the layups under tension

Layup	Material Property and Interaction	Effect Estimate [*N*]
Layup 1	X^T	13,350
Layup 2	X^T	6,670
Layup 3	S^L X^T S^L x X^T	2,670 800 670
Layup 4	Y^T S^L G_{mt} Y^T x S^L	1,300 440 110 330
Layup 5	Y^T	1,220

2.3 Sensitivity of Hashin criteria to model failure: out-of-plane bending

Following the same general procedure for the analysis of in-plane tension, the out-of-plane bending was explored with three different ply layups (layups 1–3 from Table 3). Normal probability plots of the effect estimates were used to identify significant effects, followed by smaller scale experiments to address aliasing issues, if necessary.

Ply layup 1 identified seven significant factor effects. These consisted of three positive effects and four negative effects. Removing the aliasing effects required a 2^{7-2} experiment, which indicated X^T, X^C, S^L, and the interaction of X^T and X^C as the significant properties. S^L was found to be negative and was confirmed by comparing the maximum load corresponding to the case when all properties were at nominal values to the case when just S^L was set at 20% above nominal. The comparison revealed that the maximum load decreased by almost 30% when S^L was increased by 20%.

Three effects were identified as significant for ply layup 2: the effects of X^T, X^C and the interaction of X^T and X^C aliased with the effect of the interaction between G_{ft} and G_{fc}. A 2^{5-1} (Resolution V) experiment was conducted to remove aliasing effects, which identified X^T, X^C, and the interaction between X^T and X^C to be significant material properties.

Finally, ply layup 3 identified three clearly significant factor effects, and eight that may have been significant. Resolving aliasing required a 2^{6-1} experiment, which identified only three

significant material properties: S^L, X^T, and X^C. The layup results for out-of-plane bending are summarized in Table 5.

Table 5. Summary of significant material properties and their effect on the layups under out-of-plane bending

Layup	Material Property and Interaction	Effect Estimate [N-m/N]
Layup 1	X^T	240
	X^C	180
	S^L	-200
	X^T x X^C	110
Layup 2	X^T	110
	X^C	70
	X^T x X^C	55
Layup 3	S^L	40
	X^T	40
	X^C	35

2.4 Discussion

The analyses presented in this study evaluated which material properties are most significant for the Hashin damage model used in FE models of composite panels for five simple layups loaded by out-of-plane bending and tension. For both in-plane tension and out-of-plane bending, it was determined that not all of the 10 properties are significant. Further, the results show that a small number of properties (in some cases, only one) had a significant effect on the calculated maximum load. Specifically, for the in-plane tension cases in which the ply layups had significant zero-degree plies, the tensile fiber strength was the sole significant material property. The ply layups with increasing presence of 45-degree and 90-degree plies indicated significant material properties of longitudinal shear strength and compressive strength in the in-plane direction normal to the fibers. For out-of-plane bending, layup 1 signified the expected significant properties of fiber tensile and compressive strengths, and an unexpected negative effect of longitudinal shear strength. The increased shear strength caused a stress concentration that led to an earlier damage initiation and progression.

The effects of the significant material properties on the maximum load for examined layups and loading cases are summarized in Table 6. This table shows the effect of a 20% change (+/- as

stated) in only the Hashin properties found to be significant (all other properties were unchanged) versus no change in those found to be significant and a 20% increase all others. In several cases the results are striking with the 20% change in non-significant parameters having no effect (i.e. <0.005%) on load-carrying ability. While some results might be as expected, such as X^T and Y^T being significant for Layups 1 and 2 respectively others are more likely unexpected such as the effect of S^L in Layup 3. These extreme dependencies, or lack thereof, demonstrate the potential usefulness of these loading/layup combinations for the determination, characterization, and calibration of the associated Hashin material properties.

Table 6. Summary of the effect on maximum load of significant and non-significant properties

Loading	**Layup**	**Change from all-nominal-values case**			
		+20% Significant Properties		**+20% Non-significant Properties**	
Tension	1	20.50%		11.60%	
	2	28.70%		1.60%	
	3	26.30%		5.30%	
	4	19.20%		0.00%	
	5	19.10%		0.00%	
Bending	2	25.80%		1.40%	
	3	26.80%		5.50%	
	1	+20% X^T & X^C	+20% S^L	+20% X^T , X^C -20% S^L	+20% Non-significant
		11.70%	-29.80%	69.50%	-7.20%

Of additional benefit is the methodology demonstrated. In this study the parameters associated with damage propagation, G_{ft}, G_{fc}, G_{mt}, and G_{mc}, never appeared as significant properties. This is likely because the loading/lay-up combinations selected cause sudden failure once damage is initiated and little damage propagation ever occurs. However, the study of Kennedy et al. did show parameters associated with damage propagation as significant. This suggests that thoughtful selection of loadings and layups can lead to any of the Hashin parameters being among a small number of significant properties or possibly being the only significant property. This could have a significant impact on selection of test specimens for Hashin property determination, characterization, and calibration.

3 Notched laminates subjected to mode III: out-of-plane shear loading

A considerable body of literature exists for the study of metal and composite panels subjected to mode I and mode II loading. However, mode III loading of composite panels has not been as thoroughly examined. Erdogan and Sih [11], and Sommer [12] explored mode III in brittle plates and glass, respectively. Investigators also looked at mode III loading for Plexiglas® and aluminum [13], wood [14, 15], and iron [16].

To address the composite panel deficiency, this study explored the material response of carbon fiber panels loaded in mode III. Capturing the strain fields at the tip of a notch through experimental measurements, analysis, and FE calculations were used. Specifically, the following work presents the experimental results obtained for the strain fields in notched laminates under mode III and the evaluation of the effectiveness of the commercial FE analysis package ABAQUS in predicting these strain fields.

3.1 Experimental specimens and setup

The specimens used in this study, seen in Figure 4 [17], are edge-notched, rectangular carbon fiber panels. The notch was located at the middle of the panel length and was a straight slit of 101.6 mm length, 6.4 mm width, with an end radius of 3.2 mm. The panel was 254 mm wide and 457.2 mm long. The material properties for the CFRP panels are the same as those listed in Table 1.

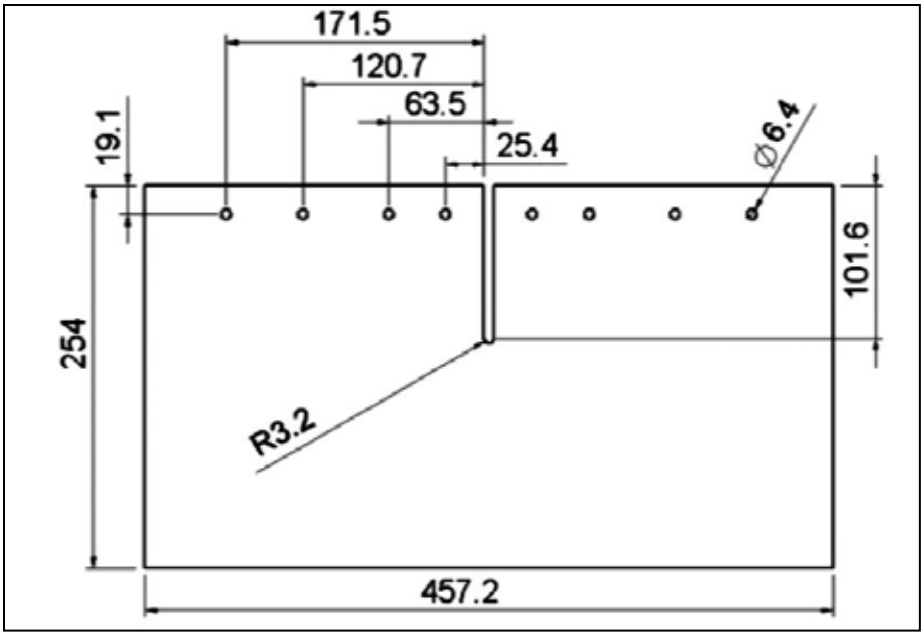

Figure 4. Edge-notched carbon fiber panel geometry (dimensions in mm)

Specimens consisted of carbon-fiber/epoxy-matrix laminates (T300/913) and contained either 20 or 40 plies. These were oriented at 0°, 45°, and 90°, with either 10%, 30%, or 50% zero-degree (0°) plies. Each ply was 0.188 mm in thickness. The panels with 20 plies in which 10% were zero-degree plies are referred to as 20-10% layup, and those with 30% zero-degree plies are referred to as 20-30% layup, with similar nomenclature for the remaining specimens.

Three panels were fabricated for each layup, and a black-on-white speckle pattern was applied around each notch tip to facilitate use of DIC Lagrangian strain measurements. Steel loading grips were attached to the panel edges by means of four screws through 6 mm holes on either side of the notch. The steel loading grips had an elastic modulus, E, of 206.8 GPa, and a Poisson ratio, ν, of 0.3.

Loading was applied through the loading grips with an Instron 5500R tensile testing machine, as shown in Figure 5 [17]. One grip was held stationary, whereas the other was displaced vertically at a constant rate of 25 mm/min to maintain quasi-static conditions. The hinge pins were unconstrained, providing a degree of freedom that prevented any significant mode I loading of the notch tip. This configuration resulted in pure mode III loading.

It should be noted that not all of the layups were symmetric. Half of the test specimens for each layup were loaded in a flipped orientation; an “even” or “odd” label is associated with each specimen for identification purposes. Whereas the load versus displacement profiles revealed the

same behavior regardless of orientation, strain fields varied between the even or odd orientation due to DIC data only being collected from the top of the specimen. For this study, the strain fields obtained from the odd orientations were used for FEA comparisons.

Figure 5. Image of specimen in loading configuration

The magnitude of the loading was quantified by the force applied to the panel edge (measured by the Instron), whereas the displacement of the panel edge (the nominal angle) was determined by:

$$\theta = 2\arcsin\left(\frac{d}{2L}\right) \tag{5}$$

where “d” is the vertical displacement of the grips (measured by the Instron), and “L” is the distance (152 mm) from the hinge pin centerline to the notch tip, as shown in Figure 6 [17].

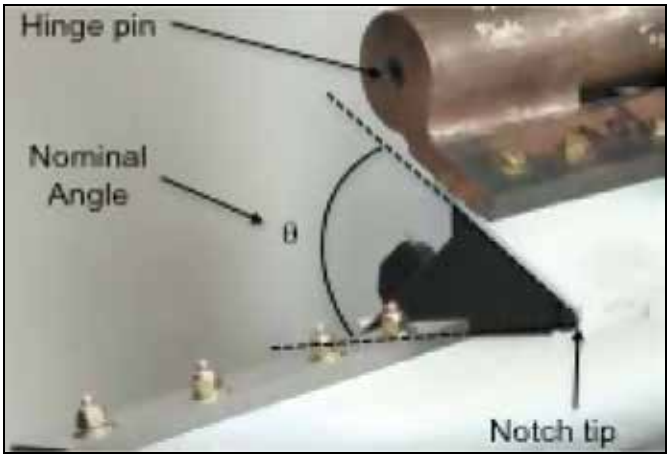

Figure 6. Image of specimen in loading configuration, with nominal angle clearly identified

The DIC images were obtained using Point Grey Research® Model GRAS-50S5M-C cameras with a shutter speed of 20 ms, lens focal length of 50 mm, and f-stop of 8. VIC-3D® software was used for all DIC calculations. DIC measurements were made at a subset size of 29 and a step size of 7, as per VIC-3D documentation recommendations.

3.2 Experimental results

Carbon-fiber/epoxy-matrix (T300/913) specimens of 20 or 40 plies, oriented at 0°, 45°, or 90°, and having either 10%, 30%, or 50% zero-degree plies at low mode III loading (3.0°), exhibited two regions of strain concentration: one tensile and one compressive. These strain concentrations of approximately equal magnitude developed primarily at the notch tip. It was observed that as the loading increased, damage began to initiate, as identified by abrupt increases of DIC-measured surface strains. For panels having fewer zero-degree plies, the increase in surface strain occurred in the tensile strain concentration area, and for panels with more zero-degree plies, increases in strain occurred in the compressive strain concentration areas. The tensile strain concentration occurred near the stationary grip, whereas the compressive strain concentration occurred near the displacing grip. Table 7 summarizes the damage initiation behavior for all of the panels studied. Note that one panel of the 20-30% layup was damaged and could not be tested.

Table 7. Summary of damage initiation for the composite panels loaded in mode III shear

Layup	Panel Number	Damage Initiation			
		Strain Concentration	Strain Magnitude	Nominal Angle	Applied Load [N]
20–10%	1	Tensile	0.043	16.7°	678
	2	Compressive	0.022	18.9°	744
	3	Tensile	0.045	19.3°	785
20–30%	1	Compressive	0.017	16.7°	643
	2	Tensile	0.042	15.1°	578
20–50%	1	Compressive	0.030	17.0°	521
	2	Compressive	0.025	15.5°	470
	3	Compressive	0.027	19.9°	632
40–10%	1	Tensile	0.028	10.5°	2043
	2	Tensile	0.039	10.5°	2080
	3	Tensile	0.030	9.7°	1934
40–30%	1	Tensile	0.040	9.7°	1800
		Compressive	0.018	9.7°	1800
	2	Compressive	0.017	7.9°	1458
	3	Compressive	0.019	8.2°	1478
40–50%	1	Compressive	0.014	9.4°	1467
	2	Compressive	0.020	9.7°	1461
	3	Compressive	0.017	9.4°	1392

As loading increased, damage began to initiate. This was first identified by abrupt increases in surface strains measured with the DIC. Increases in the tensile strain concentration areas signified initial damage in panels having fewer zero-degree plies. Conversely, increases in the compressive strain concentration areas occurred for panels with more zero-degree plies. Figure 7 Figure 8 [17] show contour plots of the average strain values around the notch tip for the 20-10% and 40-50% layups for both tensile and compressive principle strains, respectively.

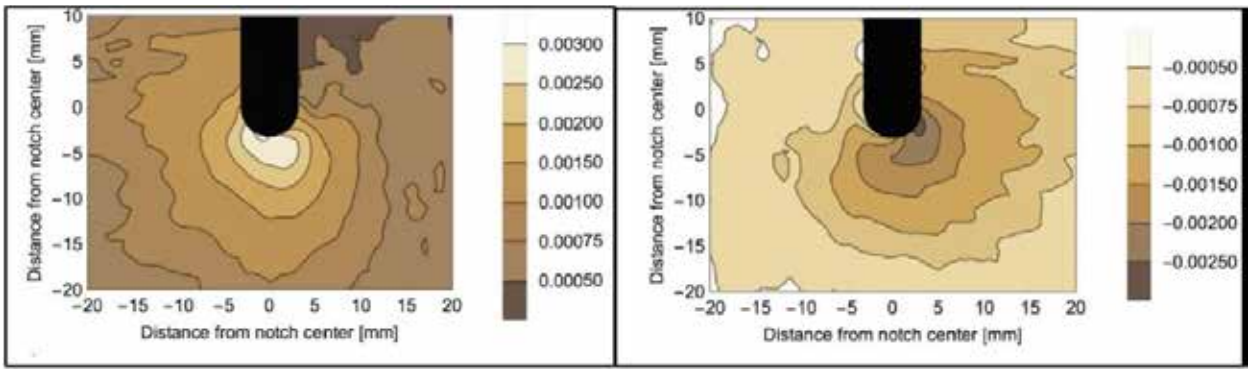

(a) (b)

Figure 7. Contour plot of average strain values around notch tip for the 20-10% layups for the (a) tensile and (b) compressive principle strains at a nominal value of 3.0° and a load of 88.5 N

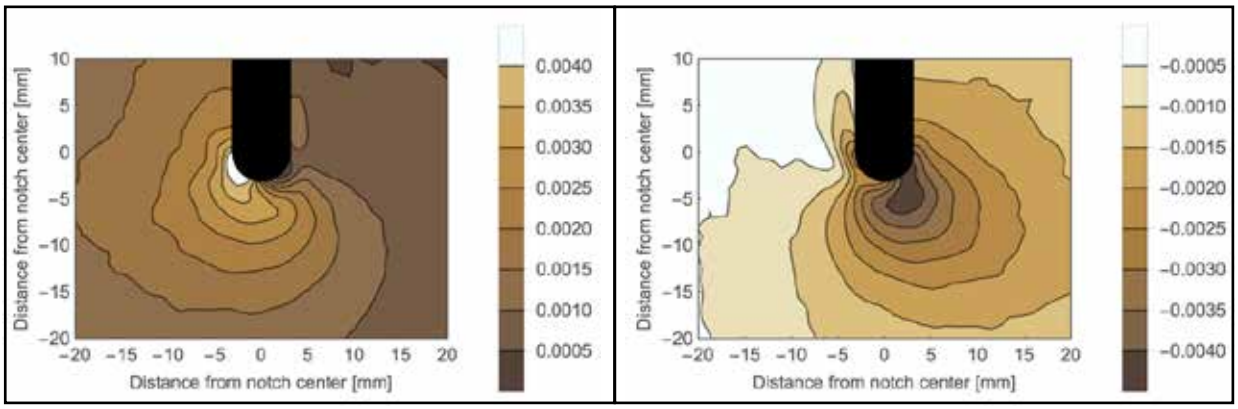

(a) (b)

Figure 8. Contour plot of average strain values around notch tip for the 40-50% layups for the (a) tensile and (b) compressive principle strains at a nominal value of 3.0° and a load of 403 N

It was concluded that DIC is effective in identifying locations of presumed internal damage where subsequent visible damage first appears. Further, this damage was shown to initiate at very small loading magnitudes. Damage concentration was shown for all panels to occur at a fairly constant strain threshold.

3.3 FEA results

A 3D ABAQUS model using ABAQUS/Standard was developed to represent the experimental configuration. The grips were modeled using eight-node reduced-integration continuum elements (C3D8R), with an element size of approximately 10.53 mm by 6.35 mm by 6.35 mm. The grip's

interaction with the panel was simulated using tie constraints on either side of the notch and along the panel length. The panels were modeled using 8-node reduced-integration shell elements (SC8R), commonly used to model composite panels. Shell elements have been shown to accurately model mode III load displacement responses of notched carbon fiber panels before the onset of extensive damage. The mesh used for all panels consisted of elements approximately 0.5 mm by 0.7 mm for a distance of 12 mm around the notch tip. After which a linearly increasing region of elements, approximately 6 mm by 7 mm, were used up to a distance of 45 mm from the notch tip. A second linearly increasing region of 18 mm by 6 mm elements were applied up to 170 mm from the notch tip.

The results of the FE model (using ABAQUS/Standard) are given in terms of percent difference from the DIC-measured values. Comparisons are constrained to within the fine-mesh region (approximately 12 mm around the notch tip) prior to damage initiation. A comparison of the 20-10% and 40-50% layups at low loading for both tensile and compressive strain fields, is shown in Figure 9 and Figure 10, respectively [17].

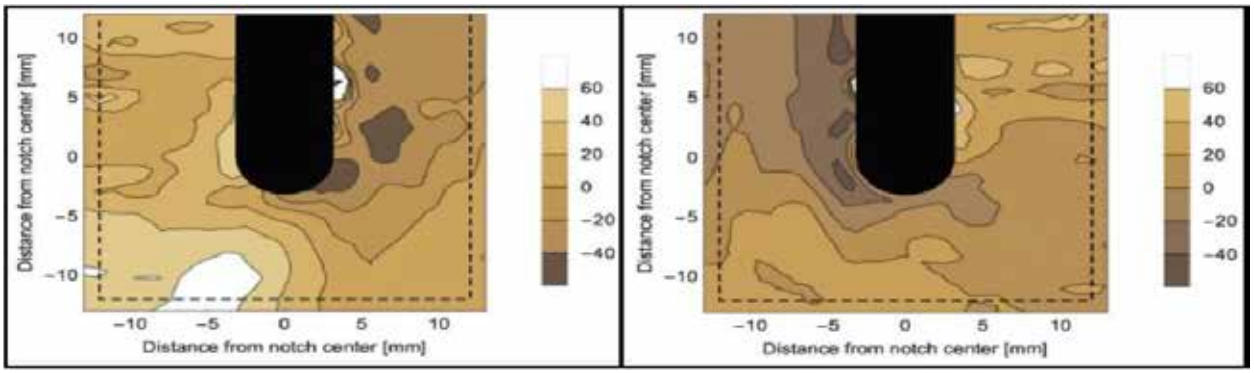

(a) (b)

Figure 9. FE model calculated strain fields at the notch tip for the 20-10% layup showing percent differences from the DIC-measured values for the (a) tensile and (b) compressive principle strains at a nominal value of 3.0° and a load of 88.5 N

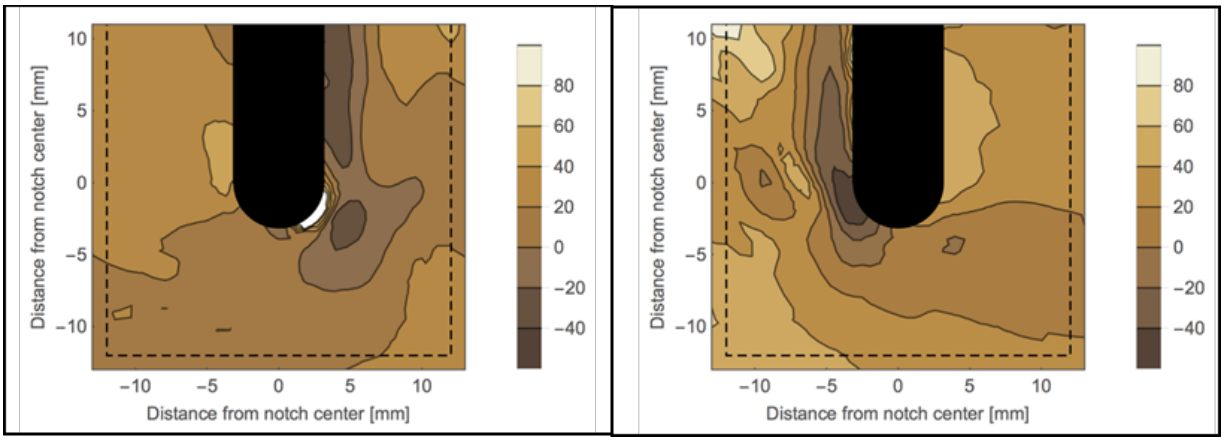

(a) (b)

Figure 10. FE model calculated strain fields at the notch tip for the 40-50% layup showing percent differences from the DIC-measured values for the (a) tensile and (b) compressive principle strains at a nominal value of 3.0° and a load of 403 N

Tensile principle strain values within the notch-tip region range between 60% higher and as much as 40% lower than measured values. For the compressive principle strains, results are similar with agreement within 20% in the area of strain concentration, with larger differences elsewhere.

For the 40-50% layup at low loading, differences between measured and simulated values ranged from near zero to 40% for tensile principle strain concentration and near zero to 20% for compressive strain concentration. All other layups exhibited similar behavior. At higher loading (nominal angles greater than 3.0°), differences of more than 100% exist between DIC-measured values and FE calculations when extensive damage accumulated.

A possible contribution to the strain value deviation may be due to the continuum shell elements not taking into account normal, out-of-plane strain. During testing, ply delamination at the notch tip was evident, likely due to out-of-plane shear.

The above strain field information was extracted prior to the onset of visible damage. All specimens exhibited damage at greater displacements. A summary of the displacement and load at visible damage initiation for all panels studied is shown in Table 8.

Table 8. Summary of initial fracture displacement and load for all layups in the study

Panel	Initial Fracture Displacement [mm]	Initial Fracture Load [N]
20 Ply, 10% 0°	45	640
20 Ply, 30% 0°	45	650
20 Ply, 50% 0°	45	520
40 Ply, 10% 0°	30	2180
40 Ply, 30% 0°	27	1880
40 Ply, 50% 0°	26	1530

From Table 8, 25 mm is the largest displacement that does not initiate damage. Therefore, the strain fields collected at 25 mm displacement were used for comparison to the simulation results.

3.4 Comparison of FEA methods

Built-in capabilities of ABAQUS/Standard, ABAQUS/Standard with Helius multi-continuum theory (MCT), and ABAQUS/Explicit were evaluated for modeling the damage progression of the experimental specimens described above. For the different FE solvers, 8-node reduced-integration shell elements (SC8R) were used to model the CFRP panels.

The Hashin damage model of progressive failure was used in ABAQUS/Standard and ABAQUS/Explicit. The material properties required for this model are summarized in Table 1. The virtual crack closure technique was also used in both ABAQUS/Standard and ABAQUS/Explicit to explore delamination. ABAQUS/Standard with Helius MCT does not use the Hashin damage model, but employs MCT and requires different material properties that are summarized in Table 9.

Table 9. Material properties required for Helius MCT

Composite Panel (Orthotropic)	General and Elastic Properties	V_f	Fiber Volume Fraction
		E_{11}	Elastic moduli in the fiber direction
		E_{22}	Elastic moduli in the transverse direction
		E_{33}	Elastic moduli in the out-of-plane direction
		v_{12}	Major in-plane Poisson's ratio
		v_{13}	Out-of-plane Poisson's ratio
		v_{23}	Out-of-plane Poisson's ratio
		G_{12}	In-plane shear modulus
		G_{13}	Out-of-plane shear modulus
		G_{23}	Out-of-plane shear modulus
		a_{11}	Longitudinal coefficient of thermal expansion
		a_{22}	Transverse coefficient of thermal expansion
		a_{33}	Out-of-plane coefficient of thermal expansion
	Strength Properties	S11 (-/+)	Longitudinal strength [compression(-) / tension(+)]
		S22 (-/+)	Transverse strength [compression(-) / tension(+)]
		S33 (-/+)	Out-of-plane strength [compression(-) / tension(+)]
		S12	In-plane shear strength [compression(-) / tension(+)]
		S13	Out-of-plane shear strength [compression(-) / tension(+)]
		S23	Out-of-plane shear strength [compression(-) / tension(+)]
	Degradation Properties	MDE	Energy-based degradation value: Matrix
		FDE	Energy-based degradation value: Fiber
		MD	Instant degradation value: Matrix
		FD	Instant degradation value: Fiber
Steel Grips (Isotropic)	Elastic Properties	E	Elastic modulus
		n	Poisson's ratio

The experimental load versus displacement profiles produced several distinct features. The profiles had an initial linear region, underwent stiffness degradation due to damage initiation and evolution, and produced a clear maximum load. The profile then underwent a progressive decrease in strength and stiffness (with increased displacement) until arriving at material failure.

ABAQUS/Standard and ABAQUS/Explicit were able to predict experimental maximum loads within 20%. Achieving a converged solution in ABAQUS/Standard required excessive hourglass stiffness scaling. ABAQUS/Explicit required excessively long run times (110 hours) and produced noisy solutions (requiring mass scaling and filtering techniques). ABAQUS/Standard with Helius MCT showed potential for modeling composites exposed to mode III shear, although the instant degradation technique led to convergence failures prior to obtaining maximum loads. Other techniques within this solver may resolve the modeling issues.

The solutions provided by all three FE solvers were able to capture the linear region, but required various techniques to obtain reasonable solutions for the damage development, maximum load, and strain softening. Additionally, ABAQUS/Standard with Helius MCT experienced convergence difficulties during the damage development while ABAQUS/Explicit resulted in high-frequency oscillations in the load versus displacement profile because of numerical instabilities. The material failure region of the profile was not accurately simulated by any of the solvers. Figure 11 [18] shows a typical load-displacement plot for experimental and all three FE solvers.

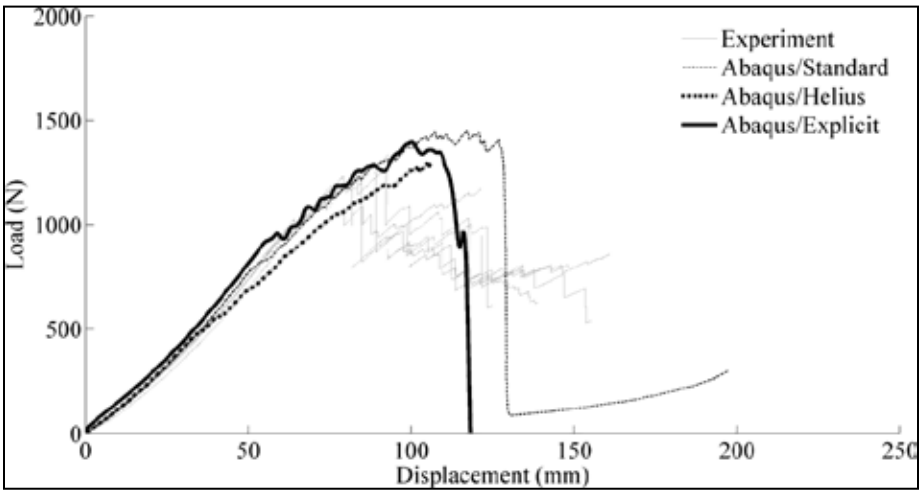

Figure 11. Load versus displacement plot for 20-10% layup for experimental and three FE solutions

4 Matrix compression propagation

The majority of the studies presented up to this point have been focused on out-of-plane bending and mode III shear, which has prompted inquiries into the damage propagation energies used as inputs of FE models. The following work investigated current FE methods used in modeling matrix compression failure.

The scope of this study had several components. First, the determination of an appropriate matrix compression testing procedure and geometry. Next, analysis using FEA was conducted, using the identified procedure and geometry to find an appropriate matrix compression propagation material model. Last, validation of the material model was undertaken using all available data and experiments.

4.1 Specimen selection through FE modeling

To explore matrix compression failure, three specimens were considered and modeled: center-notched compression (CNC), compact compression (CC), and four-point bending. Examples of the corresponding geometries are shown in Figure 12 through Figure 14 [19]. An evaluation of the specimens based on the size of the matrix compression damage zone was explored through the creation of FE models.

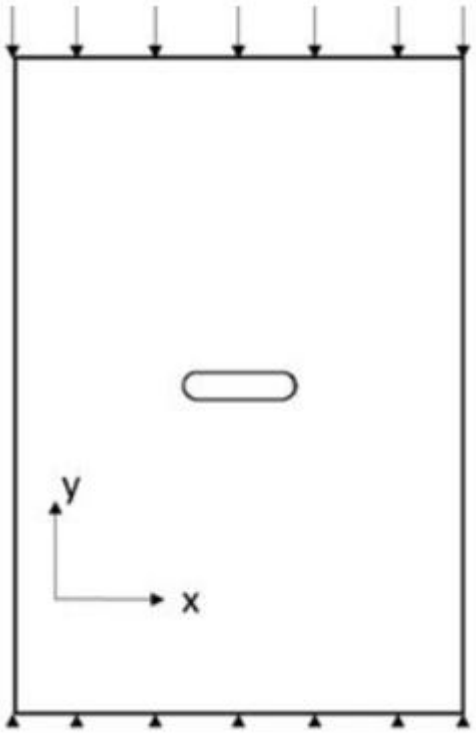

Figure 12. CNC specimen

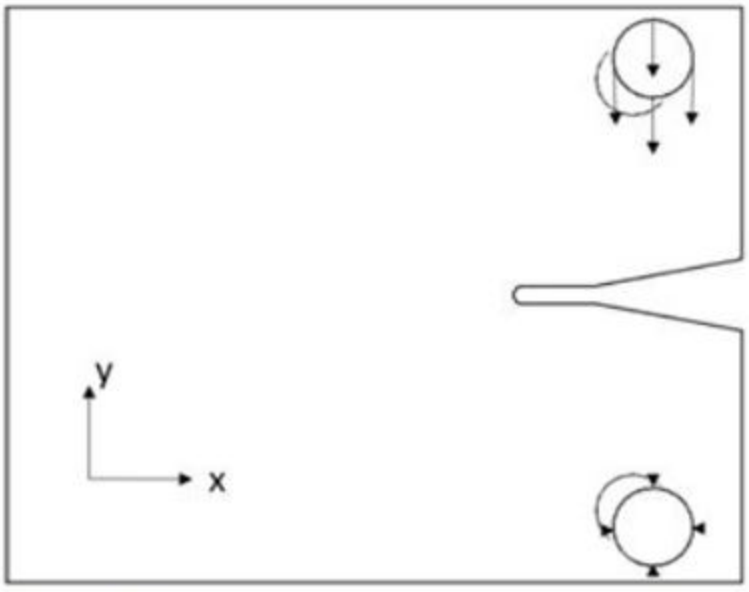

Figure 13. CC specimen

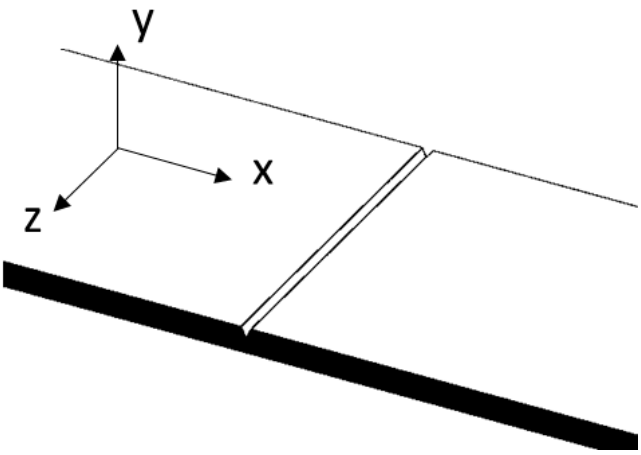

Figure 14. 4PB specimen

A necessary inclusion in the model development was the presence of anti-buckling fixtures. CNC specimens required either face-mounted or edge-mounted fixtures to prevent buckling. Use of face-mounts prevents visual monitoring of the damage area, but prevents buckling everywhere on the specimen, whereas edge-mounted fixtures only prevent buckling at the edges and provide no support for a large area of the specimen. Inclusion of these fixtures in the FE models indicated that the face mounts prevented damage propagation in the desired mode and direction. The edge-mounted fixture, however, showed good isolation of the desired damage mode. However, these specimens required complex fixtures and could be sensitive to damage growth perpendicular to the notch tip.

Modeling of the CC specimens exhibited tensile damage at the opposite end of the crack. However, compressive damage propagation occurred prior to the tensile failure. Furthermore, experimental CC specimens are easy to test and require minimal fixtures.

The 4PB FE models demonstrated significant tensile damage before compressive damage occurred. Whereas this testing fixture was readily available from a previous study, these specimens did not show good isolation of matrix compressive damage in this study.

Based on the combination of simulation results and experimental testing requirements, it was determined that the CC specimens showed the best isolation of matrix compression damage without needing fixtures as complex as the CNC specimens.

4.2 Experimental investigation of matrix compression

Preliminary tests were performed to determine the failure modes associated with the matrix under compression. Two carbon-fiber/epoxy-matrix materials were studied. The two materials were classified based on a normalized Strength Ratio calculated as the value of the matrix compressive strength divided by the matrix tensile strength. The first material is TR50S/NB301. Having the lesser magnitude Strength Ratio value, it is hereafter referred to as the “Low Strength” material. The second material is proprietary, has a comparatively greater magnitude Strength Ratio, and is thus referred to as the “High Strength” material. Unnotched specimens, comprised of 25 90°-plies, were first explored. Observations indicated that the failure was very unstable. Buckling was difficult to suppress, and the simultaneous buckling of several plies resulted in delamination. Shear cracking and damage in the matrix were also evident. Plasticity was also observed as evident by the matrix discoloration, common evidence of plastic strain in polymers.

Testing of the CC specimens, also consisting 25 90°-plies as shown in Figure 15, resulted in similar behavior to the unnotched specimens (e.g., evidence of plastic strain in the matrix, shear cracks, and delamination). The load application rate was decreased for the CC specimens to reduce global buckling but undesirable failures still occurred. Thus the CC specimen geometry needed to be altered.

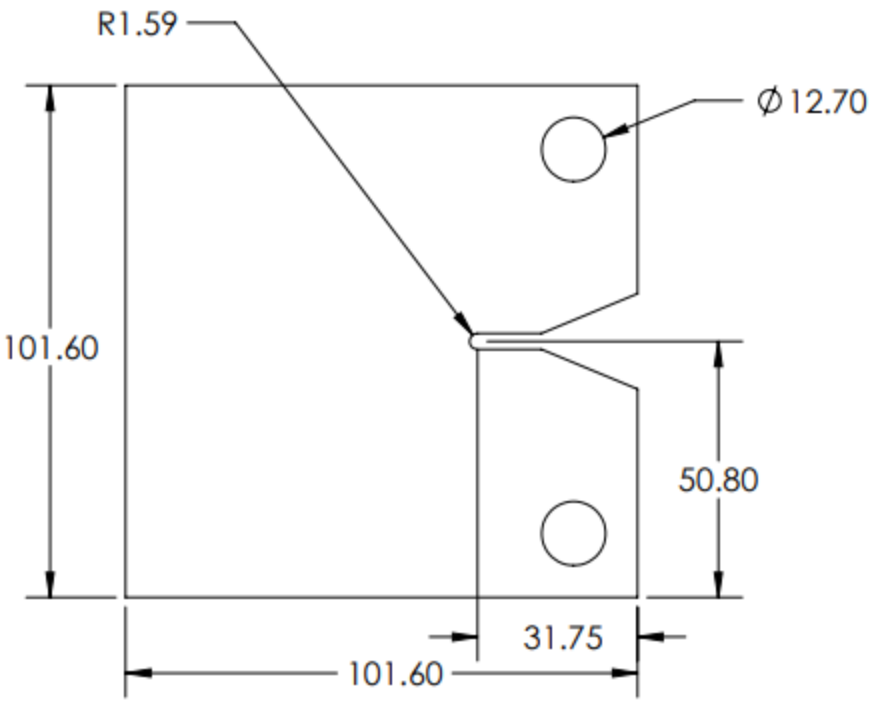

Figure 15. CC specimen (dimension in mm)

4.2.1 Experimental specimen selection

4.2.1.1 Edge notch compression (ENC) specimen

The CC specimen design went through multiple iterations starting with the edge notch compression (ENC) specimen to get the desired material failure sequence. This sequence consists of matrix-compression material failure first occurring at the notch tip (shown on the right in Figure 15) then propagating horizontally until final failure and specimen separation occurs from eventual matrix-tension material failure on the side of the specimen opposite the notch (on the left in Figure 15). The ENC specimens arose from extending the center notch compression (CNC) specimen's notch to the extreme of removing all material on one side [20]. The first iteration of the ENC specimens was manufactured from CNC specimens. The notch was extended using a 6.35-mm end mill. ENC specimens were machined to the final dimensions shown in Figure 16.

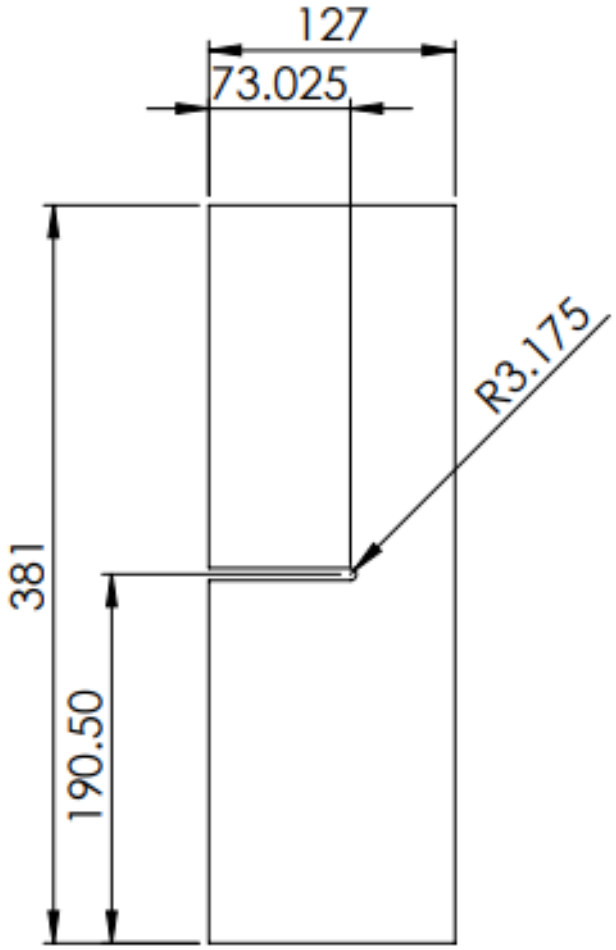

Figure 16. ENC specimen iteration 1 (dimensions in mm)

A second iteration of the ENC specimens were manufactured by modifying the previous ENC specimens. A 1.5875-mm end mill was used to decrease the radius of the notch. The notch was hand milled leading to a slight variation in length and angle as shown in Figure 17.

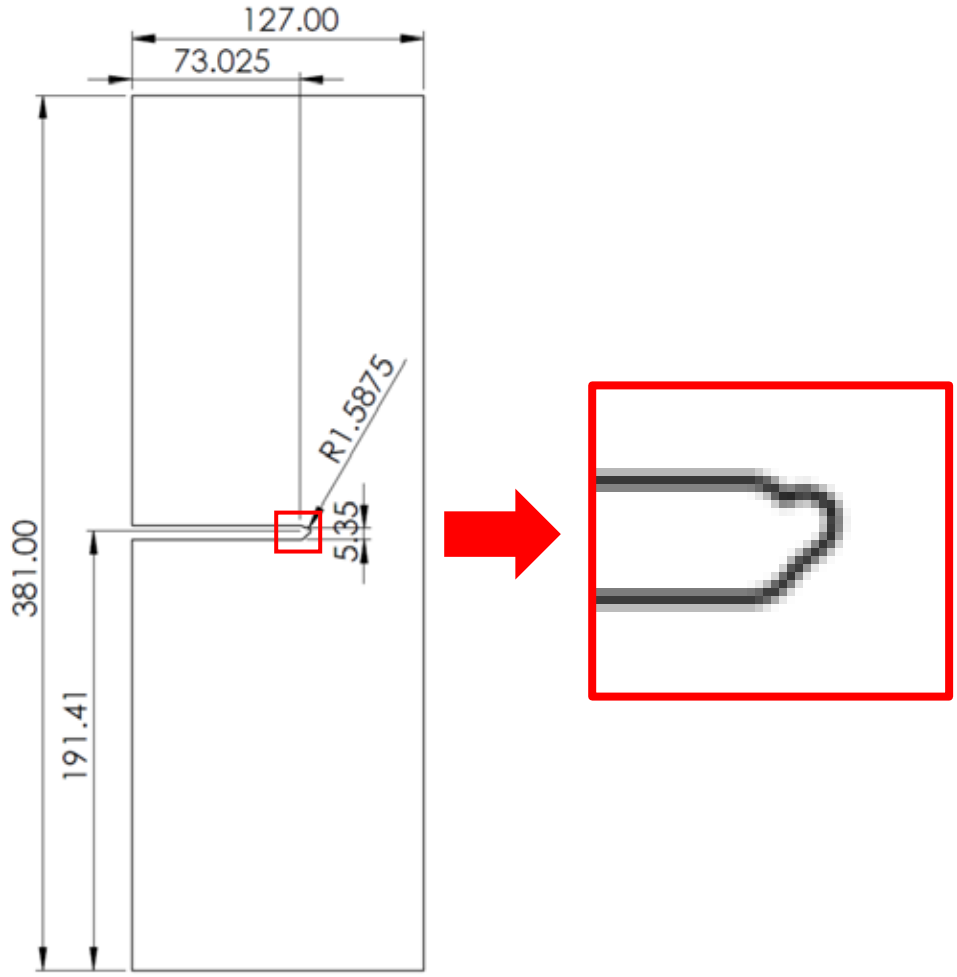

Figure 17. ENC specimen iteration 2 with the smaller milled notch shown in red box (dimensions in mm)

The third iteration of the ENC specimen were manufactured from $[90]_{25}$ 432-mm by 432-mm plates. Material within 12.7-mm of the edge of the plate was not used to ensure uniform thickness of the specimen. Specimens were water jet cut to the final geometry shown in Figure 18.

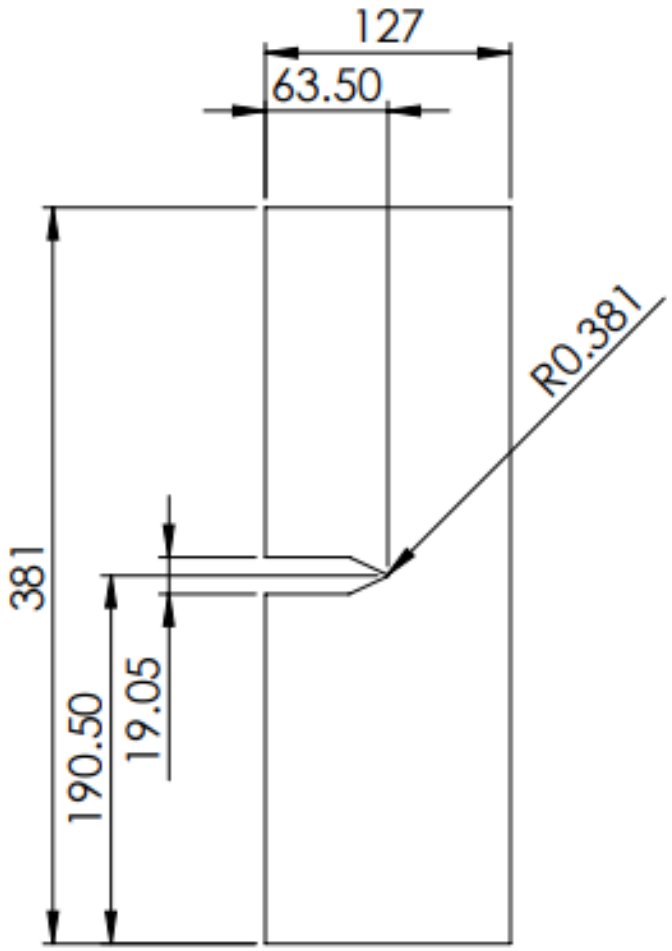

Figure 18. ENC specimen iteration 3

A 19.05-mm edge opening was used to ensure the two edges did not come into contact with each other during loading. These specimens didn't produce stable matrix-compression damage propagation as a sudden crack at the notch tip would occur followed by sudden failure on the back side of the specimen. Therefore, further specimen modification was required.

4.2.1.2 Tapered edge notch compression specimen

To account for the undesired failures of the ENC specimen, a Tapered Edge Notch Compression (TENC) was manufactured by modifying an original CNC specimen. The specimen was cut down to 177.8-mm and a taper symmetric taper was machined into the specimen with a 12.7-mm end mill. A total of three slope variations (e.g., slow variation, fast variation, and no variation) were manufactured. The slow variation TENC had a taper that reached full thickness at the edge of the specimen. The fast variation had a taper that reached full thickness at half the ligament

length. The no variation specimen had no taper and was a reduced sized ENC specimen. Figure 19 shows the final TENC specimen geometry.

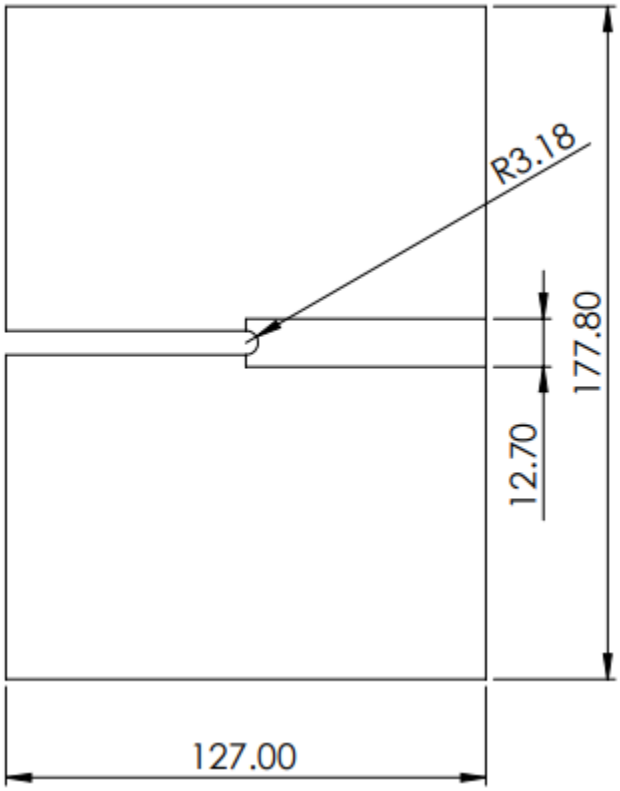

Figure 19. TENC specimen (dimensions in mm)

The slow variation TENC specimens produced an initial load drop corresponding to an initial crack propagation. After the initial load drop, the load increased again and a crack propagated through the remaining width of the specimen. A second load drop was observed after the stable crack propagation corresponding to the final fracture of the specimen. The load displacement for the slow variation TENC specimens is presented in Figure 20.

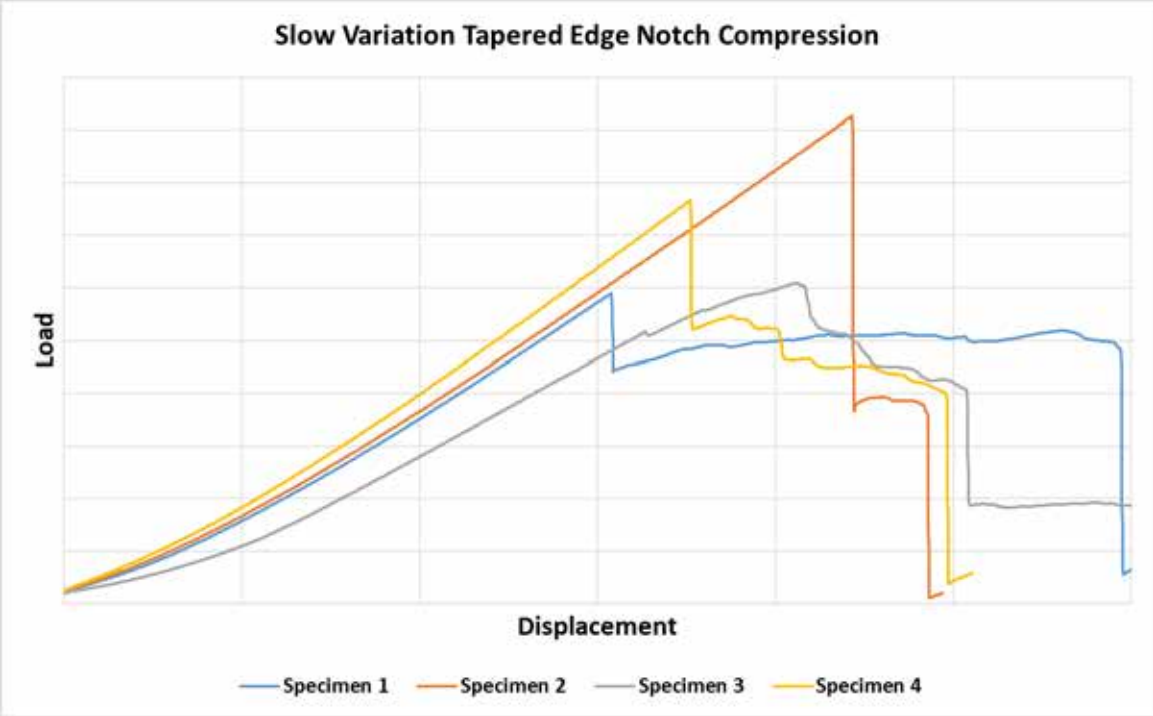

Figure 20. Load–displacement curve of the slow variation TENC specimen for high strength material (Values were omitted due to proprietary nature)

Three fast variation TENC specimens produced inconsistent failures. In two specimens, the crack formed at the edge of the machined taper and the specimens failed with a sudden crack propagation. One specimen produced an initial load drop with some crack propagation and when the crack reached the full thickness, it suddenly propagated to the edge of the specimen. The load displacement curves for the three fast variation specimens are shown in Figure 21.

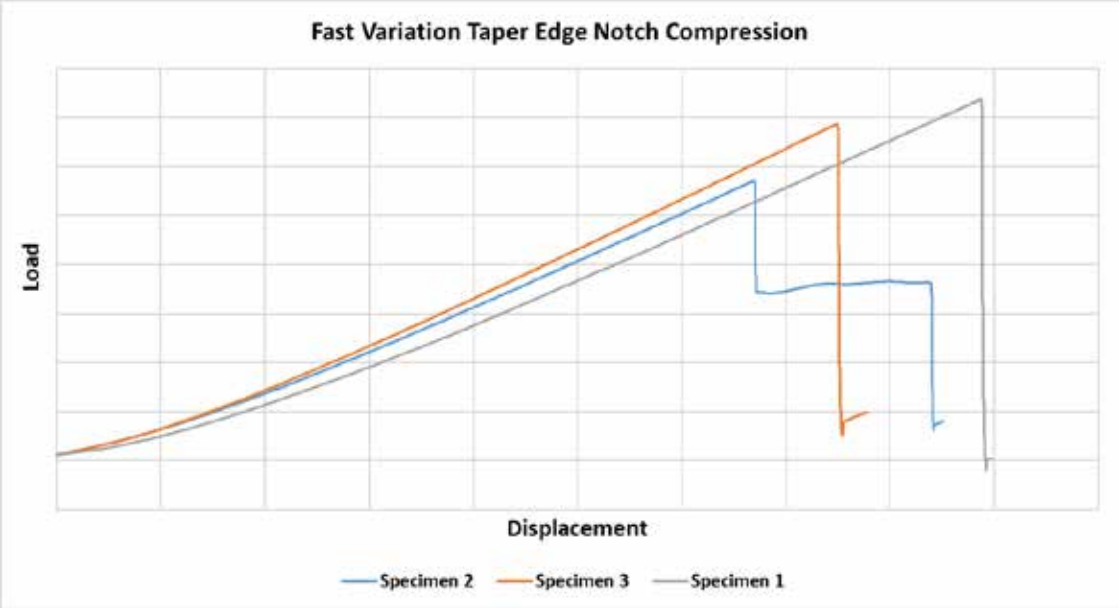

Figure 21. Load–displacement curve of the fast variation TENC specimen for high strength material (Values were omitted due to proprietary nature)

Two no variation TENC specimens produced a small load drop or non-linearity, however no significant crack propagation was observed before sudden failure. Figure 22 shows the load displacement curves of the no taper specimens.

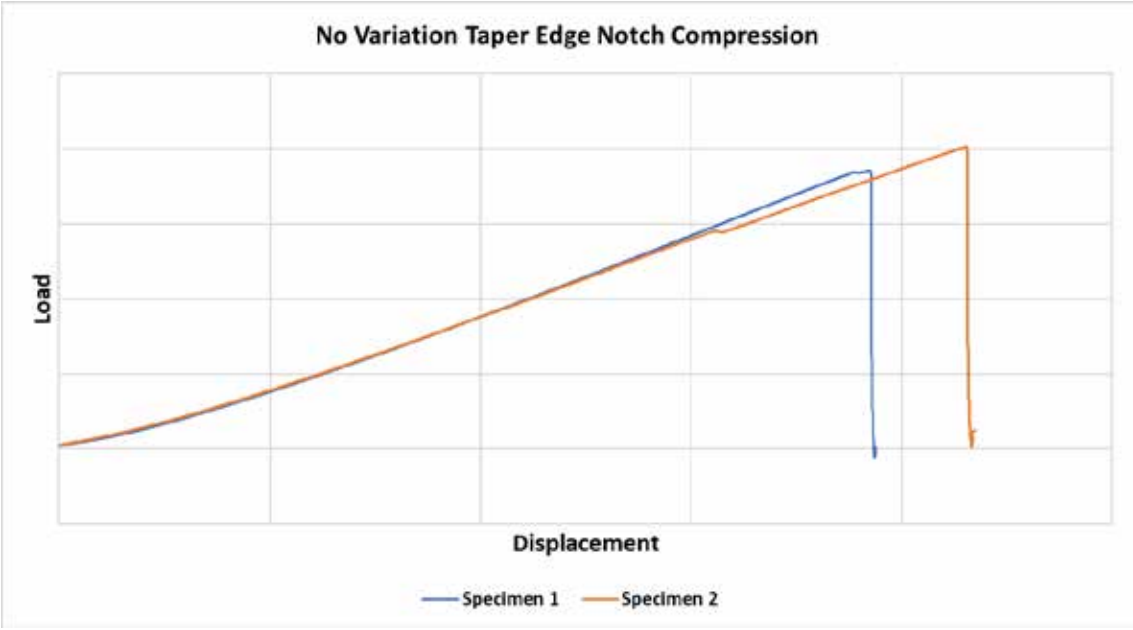

Figure 22. Load–displacement curve of the no variation TENC Specimen for high strength material (Values were omitted due to proprietary nature)

The TENC specimen experiments found that in order to induce matrix compression damage initiation and propagation, a specimen needs to have a thicker region on the back edge to prevent Euler buckling and a thinner region for the compression crack to grow. Although this specimen appeared to work, there was uncertainties relating to the specimen's need for an anti-buckling fixture and the possibility that microcracks were induced by the manufacturing process as the tapered region was machined into the specimen.

4.2.1.3 Taper layup specimen

To avoid machining-induced damages, a new 101.6-mm by 101.6-mm CC specimen was designed to have a taper as a result of the layup process. The layup schedule and ply geometry were organized to introduce a gradual taper to the specimen with a 10-ply thin region around the notch tip, and 30-ply thick region on the opposite (tensile) side of the specimen. The specimen was modelled in ABAQUS and showed promising results such as compressive damage was predicted to occur prior to tensile splitting.

Because the taper was a result of the layup schedule, and individual plies were very thin, a high-precision layup mold was designed to create the desired geometry. It is worth noting that the alignment of the top plies was difficult to achieve due to the obstruction of vision caused by the other plies. The tapered specimen shown in Figure 23 was manufactured using the low-strength ratio material as an affordable proof of concept and tested using an Instron test machine.

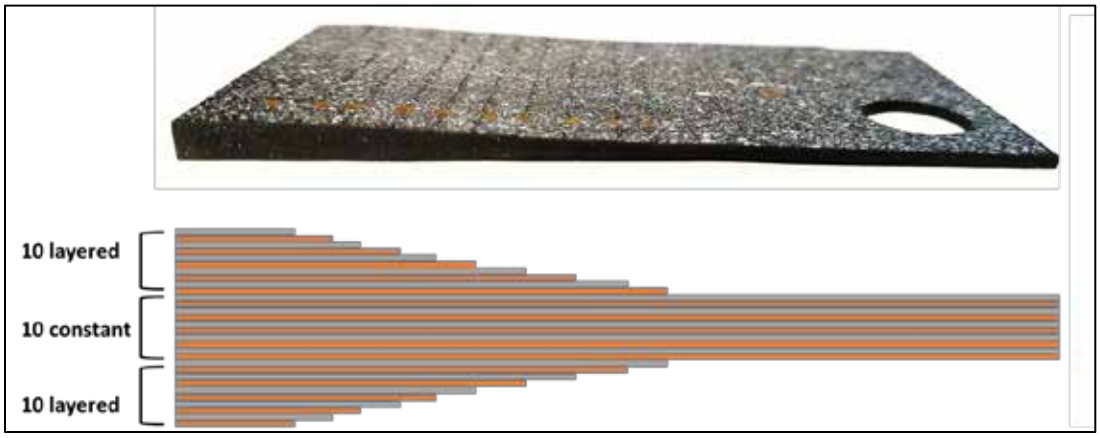

Figure 23. Taper layup specimen

The geometry of the specimen consisted of a 10-ply thin region where the load was applied, causing the specimen to buckle at this thin (compressive) side, and crack at the load application site. Any attempts to modify the mold to investigate potential solutions would require expensive

and high-precision machining. This specimen was rejected due to its manufacturing difficulties, and undesirable failure mechanism.

4.2.1.4 Machined step specimen

Because the layup taper required precision tooling and was difficult to layup, a machined step was conducted to investigate whether the specimen needed a taper, or just a thinner section. The machined step is a thin (2.03-mm) constant thickness region around the notch tip. This idea was explored by machining a step into a pre- existing, uniform thickness (4.572-mm) specimen of the high-strength ratio material using a 25.4 mm carbide end mill bit. Figure 24 shows a typical machined step specimen.

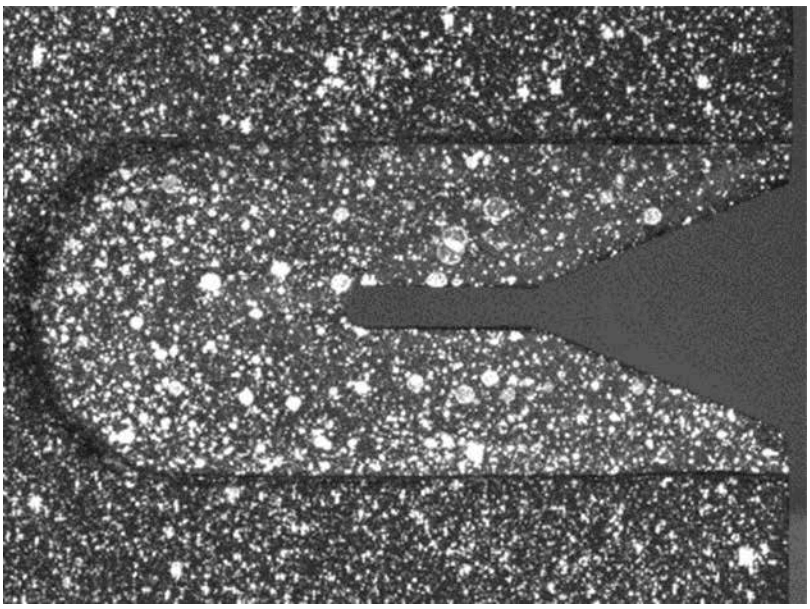

Figure 24. Machined step specimen

Testing of this specimen showed it worked and was successful in isolating compressive damage initiation and propagation, as evidenced by the sudden load drop along the linear portion of the curve in Figure 25, and the continued load-carrying ability. However, the possibility of machining-induced damages was of concern. These concerns were addressed by simply fabricating specimens having a reduced thickness (i.e., fewer plies) near the notch tip as described in the following section.

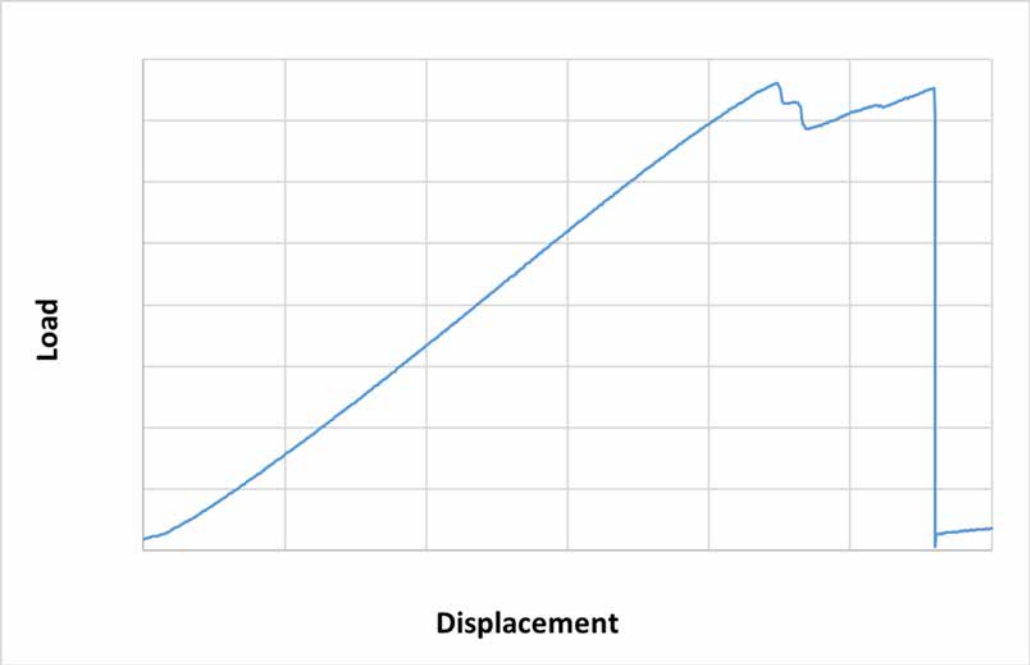

Figure 25. Load-displacement curve of the 25.4-mm machined step specimen with high strength material (Values were omitted due to proprietary nature)

4.2.1.5 Stepped compact compression specimen

The test specimen meeting all requirements and used in testing is referred to as the Stepped Compact Compression Specimen as shown in Figure 26. It consists of a 15-ply thin region around the notch tip and 35-plies elsewhere. The specimen showed successful isolation and propagation of compressive damage in the matrix for multiple notch lengths.

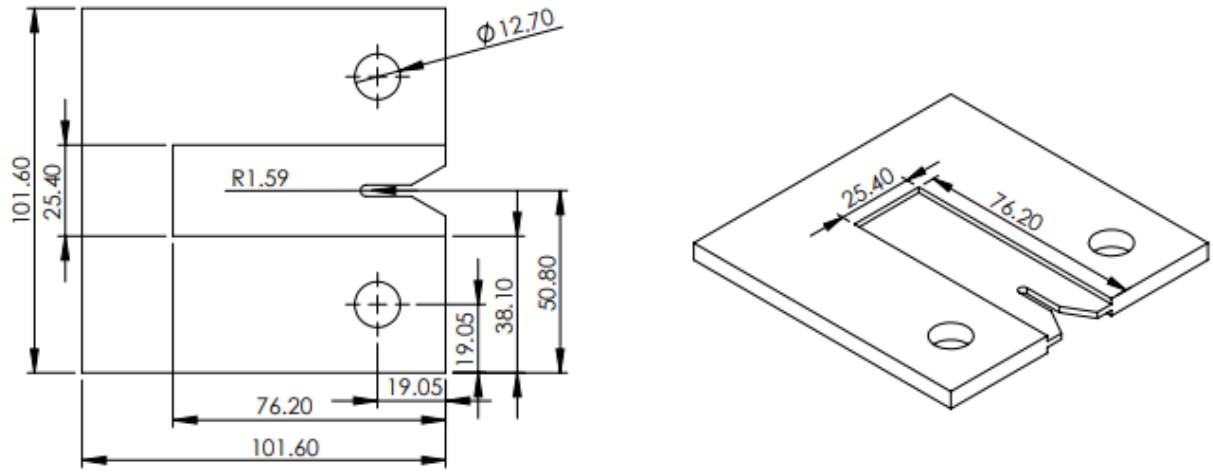

Figure 26. Stepped compact compression specimen (dimensions in mm)

4.2.2 Applicability of linear elastic fracture mechanics

Fracture mechanics involves the investigation of the failure of materials, and how to predict premature failure [21]. In a traditional (simple) approach to the strength of materials, one can relate a material's ability to withstand an applied stress to its properties (yield strength, or tensile strength). Fracture mechanics relates the applied stress to the material's fracture toughness, and a flaw size. Linear Elastic Fracture Mechanics (LEFM) is applicable to materials that obey Hooke's law, and was the foundation of the development of fracture mechanics. Under the restrictions of linear elasticity, an equation for the failure stress (or load) that a part with a crack could support was developed and is called the Griffith equation. One form of the Griffith equation is shown in Equation 6:

$$\sigma_f = \left(\frac{2E\gamma_s}{\pi a}\right)^{1/2} \quad (6)$$

Where σ_f is the applied stress at failure (the maximum stress the material can withstand until it fails), E is Young's modulus, γ_s is the surface energy of the material, and *a* is the crack half-length. Of course, Equation 6 is often generalized for any type of fracture behaviour (plastic, visco-elastic, etc.) by replacing γ_s with w_s, where w_s is the material's fracture energy. What is important to note is the dependence of the failure load to the crack half-length raised to the (-0.5) power. Recognizing that the applied stress, σ_f, is equal to the applied force divided by the area over which the force is applied, and by collecting the constant terms in Equation 6, and identifying them as C, Equation 7 can be obtained through mathematical manipulation of Equation 6:

$$\log(F_f) = C - 0.5\log(a) \quad (7)$$

Where F_f is the failure load. It is evident that a log-log plot of the failure load vs the crack half-length should yield a linear relationship with a slope of -0.5, if a material follows LEFM.

To investigate the applicability of LEFM to the TR50S/NP301 (low-strength ratio) material, specimens with the stepped geometry shown in Figure 26 were manufactured with varying initial notch lengths. Fourteen (14) different initial notch lengths were explored, with three (3) specimens manufactured for each notch length. Load-displacement curves were generated for each specimen, and image data was collected for tracking the compressive crack progression.

Using the data collected, the log-log plot discussed above was generated, and is shown in Figure 27. From this plot, a linear trend is observed with an R^2 value of about 0.83 (meaning that the linear trend line models 83% of the variability in the data), and a slope of about -0.54. A residual

plot further confirmed the appropriateness of a linear fit to the data. Although not apparent in the data collected, it is possible that as the crack length increased the proximity of the specimen boundary affected results. That is, the R^2 value and the corresponding slope value could have been affected by specimen size effects.

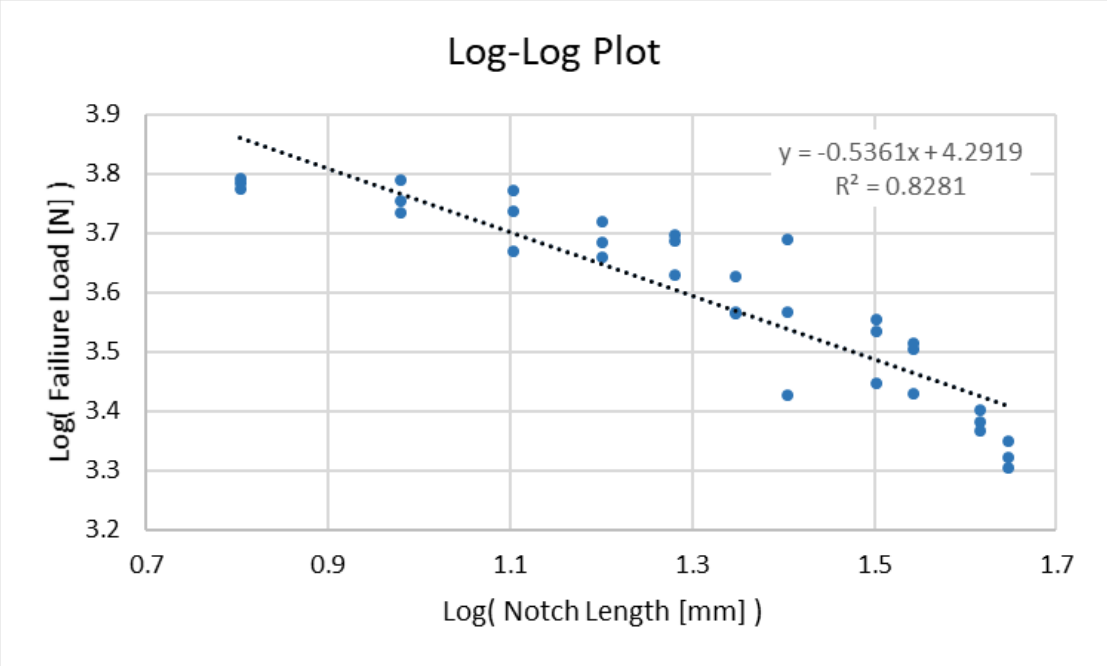

Figure 27. Log-log plot of failure load versus corresponding notch length; linear regression line is shown as dotted line with equation in upper right corner

These results clearly show that LEFM is applicable to the analysis of fracture propagation in a carbon fiber matrix under compressive loading. The linear trend observed in Figure 27 (with a slope of approximately -0.54) indicates that the matrix, under compressive loading, follows the relationship described by Equation 7, which indicates that LEFM can be applied to this material and loading. This is an important discovery allowing the powerful tools of LEFM to be used in the analysis of these materials.

4.2.3 Initial analysis of strain energy release rate

Using the test results and applying the compliance calibration method, the strain energy release rate, *G*, was calculated:

$$G = \frac{P^2}{2B}\frac{dC}{da} \tag{8}$$

Where P is the applied load, B is the thickness of the specimen, and dC/da is the change in compliance with respect to the damage length. Using equation 8, an initial value of 6.13-N-mm/mm² was calculated for the compressive damage in the matrix within the low strength (TR50S/NB301) material.

The final testing was conducted using the CC specimen geometry seen in Figure 24 [22]. The specimens were loaded with an Instron 2518-800 load cell. Use of the built-in extension and load measurements enabled the load/displacement curves to be generated.

DIC was used to measure strain and displacement fields in the material during the tests. Using two Point Grey Research® Model GRAS-50S5M-C cameras, speckle patterns on the material were tracked.

The primary failure mechanisms present in the specimens were shear cracks through the thickness of the material. Shear cracks formed at the notch tip and progressed through the thickness at angles between 47° and 57° (measured from the through-thickness direction). Other damage mechanisms began to occur as the crack propagated. Delamination of plies resulted because of the interaction of multiple shear cracks. Shear cracks began to propagate parallel to the notch, and tensile failure at the opposite end of the specimen occurred in all specimens.

4.3 Results

Through FE modeling and experimentation, multiple specimen geometries and loading configurations were explored to find a suitable candidate for matrix compression investigation. Considering the simulation results and the complexity of testing fixtures, it was determined that the Stepped Compact Compression specimens showed good isolation of matrix compression damage and stable propagation.

Figure 28 illustrates a typical load-displacement relationship. Initially load increases approximately linearly with displacement until a maximum load magnitude is reached and damage initiates. Damage initiation is immediately followed by a rapid decrease in load at a nearly constant displacement. This decrease corresponds to the sudden creation of a crack originating at the specimen's notch tip due to sudden matrix-compressive-damage growth. Following this sudden crack growth, stable growth of this crack occurs as matrix compressive damage propagates. It was observed that matrix compressive damage occurs primarily as shear cracks through the thickness of the material. Eventually the load abruptly drops to zero as the specimen fractures in two due to tensile splitting on the side of the specimen opposite the notch however sufficient data is available to determine the compressive energy absorbed in damage propagation before final failure occurs.

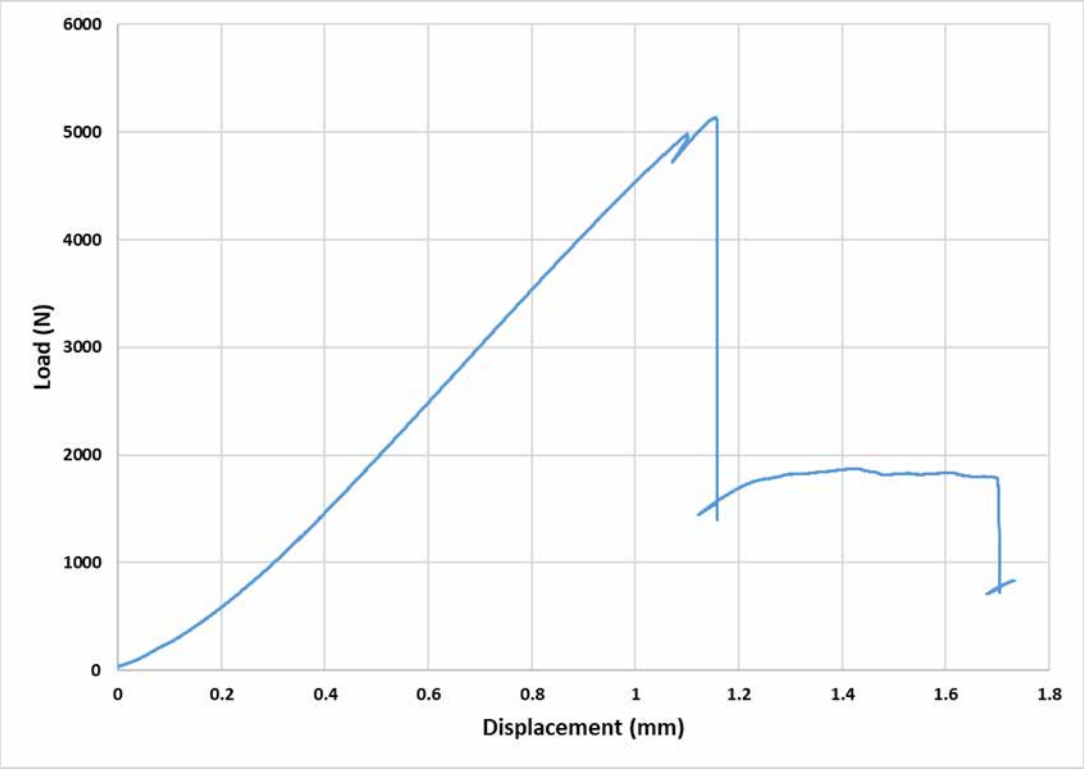

Figure 28. Typical load-displacement curve of stepped specimen for low strength material

5 Conclusion and recommendation

The objective of this research was to investigate notched laminates exposed to out-of-plane loading, and to evaluate currently existing modeling techniques and their capabilities to accurately model the failure mechanisms. The research was conducted through three investigations: 1) a sensitivity study of the Hashin criteria to model progressive damage, 2) experimental and analytical investigation of laminates under mode III shear, and 3) the investigation of composites under matrix compression. Each study produce several conclusions:

- It was determined that not all of the material properties were significant in predicting the maximum load of simple composite laminate layups under in-plane tension and out-of-plane shear. The orientation of the plies in a particular layup and the type of loading present dictates which material properties are significant for the Hashin model. In the study, as many as four material properties were significant and, in some cases, as few as one material property. Future sensitivity studies should evaluate other more complex laminate layups characteristic of wing and fuselage composite structures.

- In composite panels under mode III out-of-plane shear, it was observed that strain concentrations existed in two regions: tension and compression. Increases in the tensile strain concentration area, signifying initial damage, occurred in panels having fewer zero-degree plies. Conversely, increases in the compressive strain concentration areas occurred for panels with more zero-degree plies.
- It was also determined that results from the commercial finite element package ABAQUS were significantly different from the DIC-measured values. Differences between calculations and measured strain values were up to 60% higher and 40% lower for low loads and as much as 100% difference under greater loads.
- ABAQUS/Standard was found to be an acceptable tool to model mode III loading in composites prior to damage initiation. Although the FEA did not directly align with experimental results for mode III, it provided a good estimate.
- For progressive damage, ABAQUS/Standard and ABAQUS/Explicit were able to predict experimental maximum loads within 20%. ABAQUS/Explicit required excessively long run times and produced noisy solutions. ABAQUS/Standard with Helius multi-continuum theory showed potential, although the instant degradation technique frequently led to convergence failures prior to obtaining maximum loads.
- The study of matrix compression in CFRP panels first required the determination of a suitable test specimen. Several specimen geometries were considered. The geometry providing the needed characteristic of a significant amount of stable damage propagation was a compact compression specimen having a region of reduced thickness surrounding a notch and referred to as the Stepped Compact Compression (SCC) specimen.
- The SCC specimen was used to demonstrate that matrix compression damage propagated according to Linear Elastic Fracture Mechanics theory.
- The SCC was also used to make measurements and calculate a corresponding strain energy release rate.

Further study is recommended to evaluate matrix- compression material models currently used in finite element simulations to predict damage progression in carbon fiber laminates. The current material models used in commercial FE packages for the matrix compression behavior of carbon fiber laminates, while computationally efficient, are physically unrealistic and misrepresent material behavior and load-carrying ability. The Stepped Compact Compression test specimens can be used to experimentally define a new physically-realistic and effective matrix compression material model. Implementation of this new material model into a FE simulation to determine under what conditions (e.g. layups, part geometry, and loading) the new material model differs significantly from the currently-used material model.

6 References

1. Matzenmiller, A.J., Lubliner, J., Taylor, R.L. (1995). A Constitutive Model for Anisotropic Damage in Fiber Composites. *Mechanics of Materials, 20*(2), 125–152.

2. Hashin, Z., Rotem, A. (1973). A Fatigue Criterion for Fiber-Reinforced Materials. *Journal of Composite Materials, 7*(4), 448–464.

3. Hashin, Z. (1980). Failure Criteria for Unidirectional Fiber Composites. *Journal of Applied Mechanics, 47*(1), 329–334.

4. NASA Report. (2002). Mixed-Mode Decohesion Finite Elements for the Simulation of Delamination in Composite Materials. (NASA/TM-2002-211737).

5. Wong, K.J., Gong, X.J., Aivazzadeh, S., Tamin, M.N. (2011). Tensile behaviour of anti-symmetric CFRP composite. *Procedia Engineering. 10*, 1865–1870.

6. FAA Report. (2017). Failure of notched laminates under out-of-plane bending. (DOT/FAA/AR-11/11).

7. Wright, T.J. (2012). *Sensitivity of Hashin damage parameters for notched composite panels in tension and out-of-plane bending*. Oregon State University, Corvallis, OR.

8. Arias, S.G. (2009). *Failure Analysis of Pre-notched Composite Laminated Plates under Four-point Bending Conditions*. Oregon State University, Corvallis, OR.

9. Montgomery, D.C. (2005). *Design and Analysis of Experiments*. Hoboken, NJ: John Wiley & Sons.

10. Wright, T., Hyder, I., Daniels, M., Kim, D., Parmigiani, J. (2015). Effects of Material Property Variation in Composite Panels. *Aircraft Engineering and Aerospace Technology: An International Journal. 89*(2) 274–279.

11. Erdoga, F., Sih, G.C. (1963). On the crack Extension in Plates Under Plane Loading and Transverse Shear. *Journal of Fluids Engineering, 85*(4), 519–525.

12. Sommer, E. (1969). Formation of Fracture ‘Lances in Glass. *Engineering Fracture Mechanics, 1*(3) 539–546.

13. Jones, D.L., Subramonian, N. (1983). An Analytical and Experimental Study of the Plate Tearing Mode of Fracture. *Engineering Fracture Mechanics, 17*(1), 74–62.

14. Fruhman, K., Reiterer, A., Tschegg, E.K., Stanzl-tschegg, S.S. (2002). Fracture Characteristics of Wood Under Mode I, Mode II, Mode III Loading. *Philosophical Magazine A., 85*(17–18), 3289–3298.

15. Kamar, S.V., Srinivas, M., Rama Roe, P. (1998). Mixed Mode I/III Fracture Toughness of Armco Iron. *Acta Materialia, 46*(14) 4985–4992.

16. Barbero, E.J. (2013). *Finite element analysis of composite materials using Abaqus*. New York, NY: CRC Press.

17. Hyder, I., Froemming, T., Daniels, M., Beattie, W., Bay, B., Parmigiani, J. (2015). Mode III Loading of Composite Panels. *AIAA Journal of Aircraft, 53*(2), 343–350.

18. Hyder, I. (2014). Evaluation of Abaqus for Simulating Quasi-Static Mode III Shear of Edge Notched Carbon Fiber Reinforced Polymer Panels. Oregon State University, Corvallis, OR.

19. Daniels, M. (2016). Experimental Classification of Intralaminar Matrix Compression Damage Propagation in Carbon Fiber Reinforced Polymers. Oregon State University, Corvallis, OR.

20. Rawings, T. (2018). Experimental Specimen for Classification of Matrix Compression Damage in Carbon Fiber Reinforced Polymers. Oregon State University, Corvallis, OR.

21. T.L. Anderson, Fracture Mechanics: Fundamentals and Applications, Boca Raton, Florida: Taylor & Francis Group, 2005.

22. Carpenter, K. (2019). The Applicability of Linear Elastic Fracture Mechanics to Compressive Damage of the Carbon Fiber Reinforced Plastic Matrix. Master's Degree Thesis, Oregon State University, Corvallis, OR.